Main Manuscript for

Myosin binding protein-C limits strain induced cross-bridge detachment in response to rapid stretch in cardiac and skeletal muscle

Nichlas M. Engels[1], Rachel L. Sadler[2], Michel N. Kuehn[3,4], Devin L. Nissen[5], Dylan Reichert[6], Marius Meinhold[7,8],Wolfgang A. Linke[3], Weikang Ma[5,9,10], Anthony L. Hessel[3,4], and Samantha P. Harris[2]*

[1]Department of Cellular and Molecular Medicine, University of Arizona, Tucson, AZ

[2]Department of Physiology, University of Arizona, Tucson, AZ

[3]Institute of Physiology II, University of Muenster, Muenster, Germany

[4]Accelerated Muscle Biotechnologies, Mansfield, MA, USA

[5]BioCAT, Department of Biology, Illinois Institute of Technology, Chicago, IL, USA

[6]Department of Biomedical Engineering, University of Arizona, Tucson, AZ, USA

[7]Department of Comparative Biosciences, University of Wisconsin–Madison, Madison, WI, USA.

[8]School of Veterinary Medicine, University of Wisconsin–Madison, Madison, WI, USA.

[9]Center for Synchrotron Radiation Research and Instrumentation, Illinois Institute of Technology, Chicago, IL, USA

[10]Pritzker Institute of Biomedical Science and Engineering, Illinois Institute of Technology, Chicago, IL, USA

* Samantha P. Harris

Email: samharris@arizona.edu

Author Contributions: N.M.E, A.L.H, and S.P.H conceptualized the project, , N.M.E conducted the investigation, N.M.E visualized the datasets, S.P.H was the project administrator, A.L.H, and S.P.H supervised the study, N.M.E wrote the original draft, all authors reviewed, edited, and agreed to the final draft.

Competing Interest Statement: W.M. consults for Edgewise Therapeutics, Cytokinetics Inc. and Kardigan Bio, but these activities have no relation to the current work. A.L.H. and M.N.K. are founders and owners of Accelerated Muscle Biotechnologies, but that work is not related to the current project. All other authors declare no competing interests.

Classification:

Biological Sciences (Major)

Minor; Physiology

Keywords: myosin binding protein-C, stretch activation, cross-bridge kinetics, mouse models

This PDF file includes:

Main Text
Figures 1 to 6

Abstract

Myosin binding protein-C (MyBP-C) consists of a family of regulatory proteins expressed in sarcomeres of cardiac, fast and slow twitch skeletal muscles. The 3 MyBP-C paralogs expressed in each muscle type are encoded by separate genes but maintain a similar structure. Given the overall similarity in structure and localization of each of paralog, it is assumed that MyBP-C expressed in different muscles have similar functional effects. Here we directly tested this assumption by making use of our cut and paste approach to remove and replace N-terminal regions of MyBP-C in sarcomeres of different muscle types. We found that the different MyBP-C paralogs similarly slowed cross-bridge cycling kinetics, increased Ca^{2+} sensitivity of tension, and damped force oscillations. However, responses to a rapid stretch in actively contracting fibers, taken as indices of cross-bridge detachment and attachment kinetics, differed in each muscle type and responses depended on the presence or absence of a given paralog of MyBP-C. Altered responses to stretch were most evident for fast MyBP-C where loss of MyBP-C in psoas muscle resulted in transient responses to stretch that resembled those found in cardiomyocytes. Replacement of cardiac MyBP-C with fast MyBP-C in cardiomyocytes led to responses similar to psoas muscle. In separate X-ray diffraction experiments we also found that loss of MyBP-C in Ca^{2+}-activated psoas muscle increased lattice disorder, reduced the ordering of myosin heads, and decreased thin filament length. Taken together, these results indicate that the different MyBP-C paralogs exert both common and unique effects on myosin cross-bridge kinetics.

Significance Statement

MyBP-C is a family of regulatory proteins found in muscle sarcomeres, where they regulate contraction and relaxation. Mutations in all MyBP-C paralogs cause disease in

skeletal and cardiac muscles. We used a powerful “cut and paste” strategy to selectively remove MyBP-C from slow-twitch, fast-twitch, and cardiac muscle to show that each MyBP-C effects cross-bridge behavior similarly, though to varying degrees. Each MyBP-C had a notable effect on transient responses to rapid stretch, where MyBP-C was found to limit strain-induced cross-bridge detachment, especially in fast-twitch muscles. Strain-induced cross-bridge detachment is critical for rapid filling of the left ventricle in diastole and for sustained contraction in skeletal muscle. MyBP-C paralogs appear adapted to meet the mechanical demands of each muscle type.

Main Text

Note: Not all manuscripts need to follow the standard section order or headings outlined below. Authors are welcome to choose headings and subheadings that best fit their work. Materials and Methods should appear after the Results and Discussion in most cases.

Introduction

Myosin binding protein-C (MyBP-C) consists of a family of regulatory proteins located in sarcomeres of striated muscle. Within this family, there exist three unique paralogs of MyBP-C, each encoded by a separate gene and expressed in specific fiber types. *Mybpc1* encodes the slow twitch skeletal paralog (sMyBP-C), *Mybpc2* encodes the fast twitch skeletal paralog (fMyBP-C), and *Mybpc3* encodes the cardiac paralog (cMyBP-C)(1) The three paralogs share significant structural homology, as they all consist of a chain of 7 immunoglobulin (Ig)-like domains and 3 fibronectin type III domains termed C1-C10, a regulatory motif referred to as the M-domain, and a proline/alanine-rich domain near the N-terminus(1). Cardiac (cMyBP-C) contains an additional 8th Ig-like domain at the N-terminus termed C0 (Figure 1). Each paralog is located in the C-zone of sarcomeres, where C-terminal domains C8-C10 anchor MyBP-C to the thick filament backbone and interact with myosin heads of crown 1 and 3 in relaxed muscle(2, 3). The N-terminal

95 domains (C0-C2 for cardiac and C1-C2 for skeletal) interact with both thin and thick
96 filaments(4-7). For example, N-terminal interactions with the thin filament shift the
97 tropomyosin cable from the closed to the blocked state, thus promoting activation (i.e.
98 cross-bridge formation) in the presence of Ca^{2+} or delaying relaxation as Ca^{2+} falls(8, 9).
99 In contrast, N-terminal domain interactions with the thick filament have an inhibitory effect
100 on myosin heads by stabilizing myosin heads in the OFF state(10, 11). While less is known
101 regarding the middle domains (C3-C7) of MyBP-C, recent evidence suggests they play a
102 critical auto-inhibitory role limiting the effects of N-terminal domains to activate the thin
103 filament(12, 13). However, neither the position of the N-terminal domains nor the middle
104 domains were resolved in recent cryo-EM reconstructions and so the structural orientation
105 and interactions of these domains in the sarcomere are still unclear.

106 As evidence for MyBP-C's structural and regulatory roles in the sarcomere, mutations in
107 all three MyBP-C genes lead to disease in their respective muscle types. For instance,
108 mutations in *Mybpc3* are a leading cause of hypertrophic cardiomyopathy (HCM)(14-16),
109 while mutations in *Mybpc1* and *Mybpc2* are linked to distal arthrogryposis (DA1) and
110 myogenic muscle tremors(17-19). Although the three proteins share significant structural
111 homology, sequence homology between the paralogs is low, sharing only ~39% sequence
112 identity between the three paralogs in human muscles(20). Additionally, sMyBP-C exists
113 as a subfamily of multiple splice variants which likely have significant functional differences
114 that have yet to be thoroughly characterized(21).

115 Here we sought to compare the relative structural and functional effects of the 3 main
116 MyBP-C paralogs using our cut and paste approach to systematically remove and replace
117 MyBP-C in each of the different muscle types. The approach used 3 lines of gene-edited
118 mice, referred to as $SpyC_1$, $SnoopC_2$, and $SpyC_3$, that allow selective removal and

119 replacement of MyBP-C in slow twitch skeletal, fast twitch skeletal, and cardiac muscles,
120 respectively (Figure 1)(13, 22-24). The unique strength of these mouse models is that they
121 allow for a direct investigation of both the structural and mechanical role of MyBP-C within
122 a single fiber type, where MyBP-C can be selectively removed and replaced in a single,
123 healthy muscle fiber after it has been isolated from the animal. This is because all 3 mouse
124 lines contain a tobacco etch virus (TEV) protease recognition site followed by either a
125 short SpyTag or SnoopTag sequence between domains C7 and C8(22, 23, 25, 26)
126 (Supplemental Figure 1). Upon treatment of permeabilized muscle fibers with TEV
127 protease (TEVp), the endogenous domains C1-C7 in skeletal muscle and C0-C7 in
128 cardiac muscle are selectively cleaved and eliminated from the muscle, while domains
129 C8-C10 remain anchored to the thick filament. Following cleavage of MyBP-C, added
130 recombinant proteins containing a cognate SpyCatcher (Sc) or SnoopCatcher(SnC) form
131 a spontaneous covalent bond with the SpyTag or SnoopTag encoded at the N-terminus
132 of C8, thus permitting covalent ligation ("paste") of any desired recombinant protein *in situ*
133 at the position of endogenous MyBP-C in the sarcomere (Figure 1).

134 Using these gene-edited mouse lines, we performed permeabilized muscle mechanics to
135 measure changes in isometric force, cross-bridge cycling and stretch activation, as well
136 as small-angle X-ray diffraction to identify structural changes to the sarcomere during
137 isometric contraction. Here, we found that each MyBP-C paralog shares certain functional
138 effects including sensitizing myofilaments to Ca^{2+}, slowing cross-bridge cycling kinetics,
139 and damping force oscillations at submaximal Ca^{2+} activation. However, we found that
140 each paralog differentially regulates tension responses following a quick stretch,
141 apparently by differentially affecting strain-induced cross-bridge detachment. In psoas

142 muscle these changes correlated with increased thick and thin filament disorder during
143 half-maximal isometric contraction.

144
145 **Results**
146
147 **MyBP-C enhances Ca^{2+}-sensitivity of tension and limits cross-bridge**
148 **redevelopment rates (k_{tr}) in cardiac muscle and fast twitch and slow twitch muscles**

149 To determine the contribution of each MyBP-C paralog to function in the different muscle
150 fiber types (cardiac, fast skeletal, and slow skeletal), we first investigated the effect of the
151 different MyBP-C paralogs on steady state Ca^{2+}-sensitivity of tension as well as the rate
152 of cross-bridge cycling. Both Ca^{2+}-sensitivity and crossbridge cycling, the latter of which is
153 indicated by tension recovery from a slack-restretch maneuver, (k_{tr})(27) are both two
154 parameters that are frequently altered under disease conditions. For these experiments,
155 each MyBP-C paralog was selectively cleaved in cardiac left ventricle, fast twitch psoas,
156 and slow twitch soleus muscles from $SpyC_3$, $SnoopC_2$, and $SpyC_1$ mice, respectively, by
157 incubating permeabilized muscle fibers with TEV protease (TEVp). Results shown in
158 Figure 2 demonstrate that loss of the N'-terminal domains caused a rightward shift of the
159 tension-pCa curve, indicating reduced Ca^{2+}-sensitivity of tension such that higher [Ca^{2+}] is
160 required to achieve a given amount of force. In $SpyC_3$ cardiac muscle the pCa_{50} for tension
161 (where pCa50=-log[Ca^{+}]) was shifted from 5.401 ± 0.01 prior to TEVp treatment to
162 5.32 ± 0.01 after treatment (n=13, $p < 0.001$) (Figure 2a). Similarly, in $SnoopC_2$ fast twitch
163 psoas muscle, the pCa_{50} was shifted from 5.63 ± 0.01 to 5.57 ± 0.01, (n=10, $p < 0.001$)
164 (Figure 2b). In $SpyC_1$ slow twitch soleus we did not observe a change in Ca^{2+}-sensitivity.
165 (5.38 ± 0.02 to 5.36 ± 0.02,n=8, n.s) (Figure 2c). However, since mouse soleus muscle
166 expresses a near even mixture of slow and fast twitch fiber type populations with variable
167 MyBP-C paralogs, (28) the lack of a significant difference in Ca^{2+}-sensitivity of tension for

168 soleus muscle may reflect a relatively low proportion of sMyBP-C relative to total MyBP-
169 C. However, k_{tr} was faster at sub-maximal levels of Ca^{2+} activation in all 3 muscle types,
170 indicating an increase in cross-bridge cycling rates at these [Ca^{2+}] (Figure 2d-f). The
171 increased cycling suggests a change in either cross-bridge attachment or detachment
172 rates.

173 **Loss of MyBP-C promotes the occurrence of spontaneous oscillatory contractions**
174 **(SPOC) in all muscle types.**

175 Another common observation identified in each muscle type following cleavage of MyBP-
176 C by TEVp was the appearance of spontaneous oscillatory contractions (SPOC) that
177 became evident during Ca^{2+}-activated contraction(29). The SPOC oscillations are evident
178 as waves of contraction and relaxation that occur spontaneously, i.e., without cyclic
179 changes in activating Ca^{2+} (see Supplemental Videos 1 and 2). Recently, the SPOC
180 phenomenon has been proposed as an underlying mechanism of myogenic tremor in
181 certain skeletal myopathies linked to mutations in MyBP-C(19). We have also previously
182 reported SPOC behavior in detergent-permeabilized cardiomyocytes from $SpyC_3$ left
183 ventricles that had been treated with TEVp to remove the C0-C7 domains of cardiac
184 MyBP-C. Importantly, the oscillations were specifically due to loss of cMyBP-C because
185 they were eliminated by ligation of recombinant cMyBP-C(22). Here we investigated
186 whether SPOC is a common phenomenon following removal of MyBP-C in both slow and
187 fast twitch muscles in addition to cardiomyocytes. Figure 2g-i shows raw force traces from
188 submaximal Ca^{2+}-activated force contractions in cardiac tissue from $SpyC_3$, in psoas
189 muscles from $SnoopC_2$ mice and in soleus muscle from $SpyC_1$ mice before and after
190 treatment with TEVp. Results show that removal of C1-C7 domains from both $SnoopC_2$
191 psoas and $SpyC_1$ soleus muscle consistently resulted in robust SPOC behavior which was

192 evident as force overshoots and instabilities in the raw force traces during Ca^{2+} activation
193 (see also Supplemental videos S1 and S2). Similar to SPOC observed in cardiomyocytes,
194 SPOC in skeletal fibers occurred most commonly at submaximal [Ca^{2+}] near the pCa_{50} for
195 force generation. Therefore, MyBP-C paralogs appear critical in preventing SPOC from
196 occurring in both cardiac and skeletal muscles where undamped or prolonged SPOC may
197 contribute to muscle dysfunction in disease.

198

199 **MyBP-C paralogs differentially regulate muscle responses to rapid stretch during**
200 **Ca^{2+} activation**

201 We next investigated whether MyBP-C affects rapid tension responses following stretch
202 in Ca^{2+} activated fibers because these responses give insights into cross-bridge
203 detachment/attachment events as well as the delayed recovery of force referred to as SA.
204 For these experiments, muscles were subjected to a rapid 2% stretch relative to initial
205 muscle length followed by a 3 sec hold at the new length before returning to the initial
206 length. The resulting transient responses to the acute stretch are typically interpreted in
207 terms of cross-bridge behaviors(30, 31). As shown in Figure 3, the overall shape of the
208 resulting tension transients in response to quick stretch varied significantly depending on
209 the muscle type (i.e., responses to rapid stretch differed in cardiac, slow twitch, or fast
210 twitch skeletal muscles).

211 Figure 1 shows representative traces from cardiac muscle and psoas muscle that
212 illustrate the 3 typical phases of the transient force responses to stretch. In cardiac muscle
213 following rapid stretch there is a rapid increase in force (P_1) that coincides with and is
214 proportional to the initial stretch/increase in length. P_1 is related to both strain on bound

215 cross-bridges as well as strain on elastic elements within the sarcomere, such as titin(32).
216 Following the P_1 peak, the force drops rapidly in such a way that the rate of the decrease
217 in tension (K_{rel}) is related to the kinetics of cross-bridge detachment. Next, the nadir of the
218 tension decrease is termed P_2 and typically approaches or drops below the pre-stretch
219 steady state tension (33). Following P_2, there is a delayed rise in tension where tension
220 increases to a new steady-state value that is greater than the pre-stretch steady state
221 force (P_3). This rise to a new steady state force (P_3) termed SA (33-35), is most prominent
222 in muscles that do oscillatory work such as some insect flight muscles and vertebrate
223 cardiac muscle, whereas it is typically less prominent and shorter lived in skeletal
224 muscle(34, 36). In fast twitch skeletal muscle, the rapid increase to P1 is similar to cardiac
225 muscle. However, there is a notable difference following the initial relaxation between
226 cardiac and fast twitch skeletal muscle, where P_2 typically remains greater than the steady
227 state force prior to stretch(34). Next, instead of a delayed rise in tension to a new steady
228 state (P_3), the force briefly plateaus before slowly decreasing to a steady-state. Since the
229 fast twitch muscle tension transient typically lacks a delayed regeneration of force, the SA
230 response is considered minimal in fast twitch skeletal muscle.

231 Here, we found that the tension responses to rapid stretch were affected following removal
232 of MyBP-C in each muscle, albeit, to varying degrees. A representative trace for each
233 muscle type before and after removal of MyBP-C is shown in Figure 3. Results show that
234 removal of cMyBP-C in cardiomyocytes had overall modest effects on tension transients,
235 i.e. loss of cMyBP-C slightly reduced the P_2 nadir (by ~4% at pCa 4.5 and 5.2), increased
236 the P_{df} amplitude (P_3-P_2) by ~4% at pCa_{50}, and increased k_{rel}, the rate of relaxation
237 following the P_1 peak (97.56 ± 7.37 to 129.37 ± 8.20 at pCa_{50}) (Fig. 3d,g,j). However,
238 effects of removing fMyBP-C in psoas muscle were much more profound where tension

239 transients following loss of fMyBP-C (Figure 3b) now closely resembled a typical transient
240 response seen in cardiac muscle. That is, removal of fMyBP-C significantly decreased the
241 P_2 nadir below the pre-stretch steady state and increased the P_{df} amplitude. K_{rel} was also
242 significantly increased at sarcomere length (SL) 3.0 (Supplementary Figure 2), although
243 K_{rel} remained unchanged at SL 2.4 possibly due to a lower rate of data acquisition for this
244 data set (Figure 3e,h,k). Most strikingly, the acute removal of fMyBP-C resulted in the
245 appearance of a new delayed phase of force regeneration (phase 3) that is usually minimal
246 or absent in fast twitch fibers. This was primarily due to the decrease in P_2 because the
247 P_3 amplitudes remained unchanged in cardiac and skeletal muscle. However, the P3 does
248 appear slightly increased in the presence of fMyBP-C (Supplemental Figure 3). In slow
249 twitch soleus muscle, similar to cardiac muscle, the overall shape of the transient was not
250 dramatically changed following loss of sMyBP-C, but both the P_2 nadir decreased further
251 beyond the pre-stretch steady state, P_{df} amplitude increased, and K_{rel} rates were also
252 increased (Figure 3f,i,l). Taken together, loss of fMyBP-C conferred SA-like properties to
253 fast skeletal fibers, suggesting that canonical cross-bridge tension transient responses to
254 stretch are modulated by MyBP-C paralogs in the different fiber types.

255

256 **Skeletal muscle MyBP-C paralogs alter tension transient properties in cardiac**
257 **muscle.**

258 To directly test the extent to which differences in transient tension responses to stretch
259 are due to MyBP-C paralog expression in different muscle types, we next assessed
260 whether fMyBP-C and sMyBP-C could confer skeletal-like responses to stretch in
261 cardiomyocytes. We chose cardiac muscle as the background for paralog exchanges in
262 this set of experiments because we were able to remove nearly all endogenous cMyBP-

263 C following TEV protease treatment in cardiac myocytes compared with the more limited
264 removal of skeletal muscle paralogs from either psoas or soleus muscles that express a
265 mixture of skeletal MyBP-C paralogs (22). Additionally, because mouse hearts contain
266 primarily a single myosin isoform (α-myosin)(37), other potentially confounding effects due
267 to variable myosin isoform expression in different skeletal muscle fiber types are
268 avoided(38). Therefore, to directly assess effects of the different MyBP-C paralogs,
269 cardiomyocytes from $SpyC_3$ mice were first treated with TEVp to eliminate endogenous
270 cMyBP-C and then cMyBP-C was replaced *in situ* with either recombinant cMyBP-C,
271 fMyBP-C or sMyBP-C via SpyCatcher encoded at their C'-terminal ends. As shown in
272 Figure 5a, recombinant cMyBP-C was first added as control. Ligation of recombinant
273 cardiac C0C7Sc did not alter the overall shape of the tension transient compared to before
274 TEVp treatment, although the P_2 value tended to be higher. This could be due to the lack
275 of post-translational modifications (e.g., phosphorylation) of the recombinant C0C7Sc
276 compared to the endogenous cMyBP-C prior to TEVp treatment since phosphorylation of
277 cMyBP-C reduces P_2(39). Ligation of cardiac C0C7Sc also restored Ca^{2+}-sensitivity of
278 tension (pCa_{50}: Pre: 5.41 ± 0.01, Post: 5.32 ± 0.01, cC0C7Sc: 5.39 ± 0.02) and reduced
279 k_{tr} rates to values before treatment with TEVp (Figure 4a,d). Similar effects were observed
280 for ligation of fast C1C7Sc, where Ca^{2+}-sensitivity was restored (pCa_{50}: Pre:5.54 ± 0.02,
281 Post:5.44 ± 0.01, fC1C7Sc: 5.54 ± 0.01) (Fig. 4.b,e). However, after ligation of fC1C7Sc
282 transient responses to stretch in cardiac muscle were altered such that they more closely
283 resembled those typically seen in fast twitch skeletal fibers instead of those seen in
284 cardiomyocytes. That is, fC1C7Sc significantly elevated the P_2 amplitude above the pre-
285 stretch steady state force and nearly eliminated the rise in P_3 force (SA), leading to
286 negative P_{df} values (Figure 5e,h). Additionally, fC1C7Sc decreased the phase 2 relaxation
287 rate K_{rel}, trending to be slightly slower than endogenous cMyBP-C. (Fig. 5k). Taken

288 together, these experiments demonstrate that removal of fMyBP-C from psoas muscle
289 altered the tension transient to resemble cardiac muscle, while addition of recombinant
290 fC1C7Sc to cardiac muscle altered the tension transient to resemble fast twitch skeletal
291 muscle.

292 Similar results were seen following replacement with sC1C7Sc, which was able to restore
293 Ca^{2+}-sensitivity of tension (pCa_{50}: Pre 5.55 ± 0.02. Post: 5.49 ± 0.01, sC1C7Sc: 5.54 ±
294 0.02) and reduce k_{tr} rates to a similar extent as addition of cMyBP-C (Figure 4c,f).
295 Therefore, both recombinant fMyBP-C and sMyBP-C are sufficient to restore typical
296 interactions of endogenous cMyBP-C in cardiac muscle. sC1C7Sc also raised the P_2 nadir
297 to a level above pre-stretch steady state and nearly eliminated P_{df} amplitude of the tension
298 transient, thus significantly blunting the SA response typically seen in cardiac muscle (Fig.
299 5f,i). Taken together, these results demonstrate that skeletal muscle paralogs of MyBP-C
300 reduce canonical SA responses in cardiac muscle and instead confer skeletal-like
301 responses to rapid stretch.

302 **Structural changes following loss of fMyBP-C determined by X-ray diffraction**

303 The startling result that fMyBP-C cleavage in psoas leads to cardiac-like SA properties
304 encouraged us to identify underlying sarcomere-level structural changes. We therefore
305 used the small-angle X-ray diffraction technique on permeabilized psoas fibers from
306 $SnoopC_2$ mice under Ca^{2+}-activated conditions to determine structural changes in the
307 sarcomere before and after cleavage of fMyBP-C. In particular, we sought to determine
308 whether fMyBP-C contributed to changes in lattice spacing, lattice order, and mass
309 distributions on the thick or thin filaments that could potentially account for the change in
310 transient force behaviors described above. X-ray reflections and their relationship to

311 sarcomere structures can be visualized in the cross-sectional diagram of the sarcomere
312 (Fig. 6a,b,c).

313

314 **fMyBP-C stabilizes lattice order during isometric contraction, reduces myosin**
315 **head order, and shortens thin filament length during isometric contraction**

316 Figure 6 shows a representative X-ray diffraction pattern collected from active SnoopC$_2$
317 psoas muscle. We report on features of equatorial reflections, including the spacing of the
318 1,0 reflection (d10), the thick-filament only lattice plane spacing, and its width in equatorial
319 space, which represents the degree of heterogeneity in the lattice and thick filament
320 disorder (σ_D)(40). Under activating conditions at pCa 6.0 (approximately the pCa$_{50}$ for
321 force generation), we found that lattice spacing decreased with increasing SL as expected.
322 However, there were no significant differences in lattice spacing following removal of
323 fMyBP-C (Fig. 6d). This result differs from the increase in lattice spacing following loss of
324 fMyBP-C observed under relaxing conditions (23), but may be explained by the relatively
325 greater influence of strongly bound cross-bridges to act on the thin filament and limit lattice
326 expansion during Ca^{2+} activation. However, we found that the heterogeneity of lattice
327 spacing (σ_D) was significantly increased at both SL 2.4 and 3.0 following removal of
328 fMyBP-C (Fig. 6f). The latter suggests a modest degradation in the lattice integrity during
329 contraction when fMyBP-C is cleaved.

330 In order to further investigate the role of fMyBP-C in the orientation and order of myosin
331 heads as well as the thin filament, we investigated the $I_{1,1}/I_{1,0}$ equatorial intensity ratio and
332 M3, T3, M6 meridional reflections as well as the 6th actin layer line (ALL6) in the X-ray
333 diffraction patterns. The ratio of the 1,0 and 1,1 reflection intensities ($I_{1,1}/I_{1,0}$) reflects the

334 distribution of mass between thick and thin filaments, where increases are typically
335 associated with a shift of myosin heads to the ON state and/or binding of myosin heads to
336 the thin filament. We found that a loss of fMyBP-C did not have a significant effect on the
337 $I_{1,1}/I_{1,0}$ intensity ratio during contraction, suggesting that loss of fMyBP-C did not
338 significantly affect the distribution of myosin heads away from the thick filament backbone
339 or proportion of bound crossbridges under Ca^{2+} activated conditions. The $I_{1,1}/I_{1,0}$ intensity
340 ratios at both short and long SL (SL 2.4 and 3.0) also remained unchanged during
341 isometric contraction, as previously reported by others (41, 42). Next, the spacing of the
342 M3 reflection (S_{M3}), a measure of the axial periodicity of myosin heads, did not significantly
343 change at either SL 2.4 or 3.0 following loss of fMyBP-C (Supplementary Figure x).
344 Because S_{M3} is also taken as a measure of whether myosin heads are primarily in the OFF
345 or ON state, results suggest that fMyBP-C does not contribute significantly to the OFF/ON
346 distribution of myosin heads or numbers of bound myosin heads under active conditions,
347 consistent with the $I_{1,1}/I_{1,0}$ intensity ratio. The intensity of the M3 reflection (I_{M3}), however,
348 decreased following removal of fMyBP-C (Figure 7g), consistent with an increase in the
349 angular dispersion of myosin heads(43, 44), suggesting that loss of fMyBP-C promotes
350 disorder of myosin heads. The spacings of other thick filament reflections, such as (S_{M6}),
351 indicative of thick filament length, were unchanged following removal of fMyBP-C
352 (Supplementary Figure 4).

353 Finally, we sought to determine whether any thin filament structural changes occurred
354 following fMyBP-C removal. We found that the spacing of the third-order troponin reflection
355 (S_{T3}) was significantly decreased following removal of fMyBP-C at both SL 2.4 and SL 3.0,
356 suggesting a reordering of the troponin complex on the thin filament. Additionally, the
357 spacing of actin layer line 6 (S_{ALL6}), reflecting the pitch left-handed helix of actin, was

358 significantly decreased following removal of fMyBP-C at both SL 2.4 and SL 3.0 μm (Fig.
359 6i).

360
361 **Discussion**
362
363 **Myosin binding protein-C paralogs commonly influence Ca^{2+}-sensitivity, cross-**
364 **bridge cycling, and oscillatory contractions in striated muscles**

365 In this study, we sought to identify key similarities and differences in the role of the three
366 major MyBP-C paralogs in regulating muscle contractility, as well as identify key roles for
367 fMyBP-C in the structural organization of isometrically contracting sarcomeres. Using
368 three genetically modified mouse lines specific to slow ($SpyC_1$), fast ($SnoopC_2$), and
369 cardiac-MyBP-C ($SpyC_3$) that allow for selective removal of MyBP-C and replacement with
370 recombinant MyBP-C in the respective muscle types, we were able to test mechanical
371 properties of each muscle type in the presence and absence of MyBP-C. We found that
372 selective cleavage of MyBP-C led to a reduction in Ca^{2+}-sensitivity in both cardiac and fast
373 twitch myocytes. Effects on Ca^{2+}-sensitivity did not reach significance in soleus, a
374 predominantly slow twitch muscle, likely due to significant co-expression of fast and slow
375 MyBP-C (since fMyBP-C would not be cleaved in skeletal muscles from $SpyC_1$ mice).
376 However, recombinant slow MyBP-C was able to restore Ca^{2+}-sensitivity when added to
377 $SpyC_3$ cardiac myocytes (Figure 4f), so all 3 paralogs apparently share the common ability
378 to shift the tension-pCa relationship to the left. Similarly, cleavage of each MyBP-C paralog
379 increased cross-bridge cycling rates at submaximal Ca^{2+} activation as measured by k_{tr}.
380 This result is in good agreement with previously reported changes in both cardiac and fast
381 skeletal MyBP-C KO mice as well as previous work with the $SnoopC_2$ and $SpyC_3$ mouse
382 lines(22, 45, 46). Moreover, loss of each MyBP-C paralog led to the appearance of
383 spontaneous oscillatory contractions at sub-maximal Ca^{2+} activations near the pCa_{50} for

384 force generation. While the precise mechanisms by which oscillatory contractions are
385 induced and propagated are still unclear, the phenomenon is an intrinsic, emergent
386 property of sarcomeres that has been likened to a third state of muscle activity between
387 activation and relaxation(29, 47). Notably, because force oscillations occur at Ca^{2+}
388 concentrations expected to be encountered in living muscle and are influenced by
389 metabolites such as ADP/P_i(48), tension instabilities are likely to have physiological
390 relevance. Consistent with this idea, mutations in slow MyBP-C lead to force oscillations
391 that are associated with skeletal muscle tremor in humans(17, 49, 50). Results presented
392 here therefore suggest that a novel functional role of all 3 MyBP-C paralogs is to limit
393 mechanical force instabilities and promote contractile synchrony. Conversely, loss of
394 MyBP-C or mutations in MyBP-C underlie contractile dysfunction in different muscle types
395 (51).

396 **Myosin Binding Protein C paralogs differentially contribute to tension transients in**
397 **striated muscle**

398 While we identified several common functional effects of the different MyBP-C
399 paralogs as discussed above, a notable departure from this trend was evident when
400 comparing the differential responses to a rapid 2% stretch in each muscle type which we
401 found were attributable to expression of the different MyBP-C paralogs. For instance,
402 under control conditions all 3 muscle types (cardiac, fast and slow skeletal) had unique
403 responses to rapid stretch that were mostly stereotypical for that muscle type as previously
404 described by others(19, 33, 34, 52, 53). This was most evident when comparing the
405 responses of cardiac and psoas (fast skeletal) muscles, where cardiac muscle exhibited
406 a canonical 3 phase response that included a final phase such that after reaching a nadir
407 (P_2), steady state force rises above the pre-stretch force, P_3. (SA, discussed in more detail

408 below). By contrast, P_2 was highly elevated in psoas muscle and the phase 3 rise in force
409 was typically minimal and/or short-lived. Notably, classical SA behavior is generally
410 considered minimal or absent in fast twitch muscle, although enhancement of SA in
411 skeletal muscles may be important under conditions of fatigue (e.g., high inorganic P_i) (34,
412 52, 54). Strikingly, as shown in Figure 3, we found that loss of fMyBP-C after TEVp
413 cleavage in psoas muscle completely altered the stereotypical response to stretch and
414 completely converted the response into one resembling that of cardiac muscle, including
415 a significant decrease in P_2 and the appearance of a prominent phase 3 SA (delayed force
416 increase) response. Conversely, when fMyBP-C was added to cardiac myocytes (Fig. 5),
417 the tension transient converted into a response more closely resembling one typically
418 found in fast skeletal muscle where P_2 was elevated and phase 3 was eliminated. Taken
419 together, our results provide compelling evidence that the different MyBP-C paralogs
420 contribute significantly to the stereotypical tension transient responses in their respective
421 muscle types. Furthermore, to our knowledge, this is the first report showing that loss of
422 fMyBP-C confers classic SA-like properties to fast twitch skeletal muscle fibers.

423 Tension transient responses to stretch, including SA responses, are thought to be
424 mediated largely by changes in cross-bridge cycling kinetics (30). Accordingly, numerous
425 factors that are known to impact cross-bridge dynamics, including calcium, ADP, and P_i
426 concentration, the extent of stretch, temperature, and the contribution of other sarcomere
427 proteins, such as thin filament proteins as well as myosin heavy chain isoforms, have all
428 have been shown to significantly impact the shape and rate of tension transient responses
429 to stretch(34, 54-56). In this respect, it may not be surprising that MyBP-C, known to affect
430 cross-bridge cycling kinetics, also influences tension transients. Indeed, consistent with
431 results reported here, Stelzer et al (2006) reported increased K_{rel}, reduced P_2, and

432 increased K_{df} rates in cMyBP-C KO mice, effects that were largely replicated by PKA
433 phosphorylation of WT cMyBP-C (33, 39). PKA phosphorylation of sMyBP-C in slow twitch
434 fibers also increased force development rates (57). Our results thus confirm and extend
435 previous findings by showing that all 3 MyBP-C paralogs limit cross-bridge cycling kinetics
436 in their respective muscle types. However, to further explore the extent to which each
437 paralog by itself was sufficient to determine the overall shape of tension transients when
438 expressed in a similar background, we also utilized the $SpyC_3$ cardiac mouse line that
439 primarily expresses a single myosin isoform (α-myosin) in cardiac myocytes to
440 systematically replace endogenous cMyBP-C with recombinant cardiac, slow , and fast
441 MyBP-C. Again, we found that each MyBP-C paralog conferred a characteristic tension
442 transient in cardiac muscle, thus allowing us to attribute observed changes in the tension
443 transients primarily to the different paralogs of MyBP-C rather than to different myosin
444 isoforms or other confounding variables.

445 **MyBP-C paralogs determine the extent of strain-induced cross-bridge detachment,**
446 **P_2**

447 A key difference that emerged when comparing the tension transients in the different
448 muscle types was the extent of the P_2 nadir, which presumably reflects the magnitude of
449 cross-bridge detachment in response to strain in each muscle type. Notably, P_2 was
450 reduced following loss of MyBP-C in all 3 muscle types, suggesting that a normal function
451 of MyBP-C is to limit strain-induced cross-bridge detachment. In cardiac muscle, strain-
452 dependent cross-bridge detachment is emerging as a key regulator of the mechanical
453 control of relaxation where stretch enhances LV relaxation during the transition from late
454 systole to early diastole(55, 58, 59) . In fact, Stehle et al. concluded that load-dependent
455 cross-bridge detachment is the only mechanism that explains how cardiac muscle can

456 relax as quickly as it contracts(60). Consistent with this, small stretches during the slow
457 phase of myofibril relaxation were shown to accelerate the onset of sarcomere "give"
458 which initiates the fast exponential phase of relaxation(61). We also recently showed that
459 loss of cMyBP-C significantly accelerates the fast phase of relaxation suggesting that
460 cMyBP-C provides an internal load (potentially by cross-linking thick and thin filaments) or
461 otherwise stabilizes sarcomere dynamics to slow relaxation(24).

462 In fast skeletal muscle acceleration of strain-dependent cross-bridge detachment after
463 loss of MyBP-C may contribute to the appearance of SA-like properties. For instance,
464 Wakefield et al. modeled cardiac tension transients in terms of a model where the shape
465 of the transient was the sum of 3 main factors: a passive Power-law relaxation term, a
466 Reversal term that is responsible for the transient drop in force (P_2 nadir), and a Drag term
467 that represents the initial fast rise in tension and relaxation immediately after the
468 stretch(59). If the Reversal term in skeletal muscle is small as suggested by Davis and
469 Epstein(32), and further limited by MyBP-C, then the shape of the tension transient in
470 skeletal muscle would be expected to be dominated by a combination of the Drag and
471 Power-law terms. However, if loss of fMyBP-C increases strain-dependent cross-bridge
472 detachment (g_1 in their model), then the Reversal term would become greater and deepen
473 the amplitude of the P_2 nadir(59). At the same time, loss of MyBP-C could further reduce
474 the Drag term as well as leading to an overall increase in the R/D ratio. Together, the two
475 effects would lead to the appearance of an SA response as observed following the loss of
476 fMyBP-C.

477 Through which interactions are the various MyBP-C isoforms able to affect the Drag and
478 Reversal terms? If MyBP-C links the thick and thin filaments and is able to slow filament
479 sliding(45, 57), then this interaction would be expected to increase the Drag term. MyBP-

480 C's presence may also limit the Reversal term, for instance, by preventing P_i-dependent
481 reversal of the powerstroke. Consistent with this cMyBP-C slows phosphate (P_i)-
482 dependent myosin cross-bridge detachment and prolongs cross-bridge lifetimes in cardiac
483 muscle (62, 63). Tanner et al. further concluded that cMyBP-C inhibits P_i-dependent
484 reversal of the powerstroke or otherwise stabilizes cross-bridge attachment in a way that
485 increases the probability of myosin completing its powerstroke(64). Notably, to account
486 for differences in relative rates of P_2 ($P_{2\text{-slow}}$) in different fiber types, Davis and Epstein
487 argued that P_i-dependent reversal of the powerstroke is largely absent in fast fibers,
488 whereas it is prominent in slow fibers(32). Straight et al. also concluded that a reverse
489 stroke of slow skeletal myosin accounts for augmentation of SA in slow skeletal muscle,
490 but not in fast skeletal muscle(34), although the same group later found that increases in
491 [P_i] concentration, such as during muscle fatigue, augments SA even in fast twitch
492 fibers(54). Using optical tweezers and synthetic cardiac myofilaments, Hwang et al.
493 demonstrated that a reversal stroke is present in cardiac myosin, but absent in fast skeletal
494 myosin, where it is a key determinant of cardiac contraction and relaxation and is further
495 necessary to produce stable force even at low levels of Ca^{2+} activation(65). While the
496 reversal stroke (or absence of) is therefore likely intrinsic to the myosin isoform, our results
497 suggest that MyBP-C paralogs are key regulators of cross-bridge detachment rates,
498 potentially via modulation of P_i-dependent reversal of the powerstroke(66).

499 SA is a phenomenon best described in some insect flight muscles that operate at high
500 frequencies (100-1000 Hz) where muscle is turned on and off in response to mechanical
501 signals rather than being driven by slower and more energetically costly chemical and
502 electrical signals(35, 67, 68). In these so-called asynchronous muscles, a single action
503 potential elicits a sustained rise in [Ca^{2+}] that is permissive for multiple cycles of muscle

504 activation and relaxation driven by muscle stretch. The initiating mechanical event, muscle
505 stretch, itself is the result of contraction of an antagonistic muscle such that asynchronous
506 muscles act in pairs. By accelerating strain-induced cross-bridge detachment, it is
507 plausible that stretch synchronizes relaxation of a population of cross-bridges that contract
508 together resulting in SA. In this respect it is notable that MyBP-C, which appears to limit
509 strain-induced cross-bridge detachment as we show here, is absent in insect flight
510 muscles, although other proteins such as projectin and flightin may perform analogous
511 roles(69-71). While mammalian cardiac and skeletal muscles utilize a synchronous
512 contractile mechanism (where a single action potential leads to a single twitch), SA occurs
513 to some extent in both muscle types and may play important physiological roles. Examples
514 include coordinating proper ejection timing of the ventricle and mechanical control of
515 relaxation in the heart (55, 58, 72), or during exercise where contraction of one muscle
516 may lead to stretch in its antagonistic partner, priming it for contraction moments later(52,
517 54). Our results suggest that by modulating strain-dependent cross-bridge detachment
518 MyBP-C fine-tunes the contribution of SA in different muscle types and that regulation of
519 MyBP-C, for instance by phosphorylation within a given muscle type, may thus contribute
520 to a greater or lesser dependence on mechanical signals for activation and relaxation(33,
521 57).

522 **Potential mechanisms for MyBP-C regulation of the tension transient response**

523 To gain additional insights into mechanisms by which loss of MyBP-C affects cross-bridge
524 kinetics, we investigated structural effects of loss of MyBP-C using X-ray diffraction
525 analyses of Ca^{2+}-activated psoas muscle before and after cleavage of MyBP-C with TEVp.
526 We chose psoas muscle for X-ray diffraction studies because the effects of loss of MyBP-
527 C were greatest in psoas muscle (e.g., the reduction in P_2 was greatest) and because we

528 had previously characterized loss of MyBP-C in psoas muscle under relaxed
529 conditions(23). In that study we found that loss of MyBP-C expanded the sarcomere
530 lattice, reduced the length of the thin (actin) filament, and repositioned myosin heads from
531 their OFF to ON positions on the thick filament. These results were overall consistent with
532 effects of MyBP-C to stabilize the inhibited state of myosin and limit lattice expansion
533 potentially through interactions of MyBP-C with actin. By contrast, here we found under
534 Ca^{2+}-activated conditions that loss of MyBP-C did not significantly affect lattice spacing
535 possibly because strongly bound cross-bridges effectively limit the separation of the thick
536 and thin filaments. However, an indicator of lattice disorder or heterogeneity, σ_D, was
537 significantly increased at both SL 2.4 and SL 3.0 μm following loss of MyBP-C. Palmer et
538 al., also reported greater myofilament disorder in a mouse model of cMyBP-C
539 knockdown(63). σ_D is increased during active conditions compared to passive conditions,
540 likely due to contributions of cross-bridge cycling that tend to move the positions of both
541 thick and thin filament relative to their equilibrium position in the lattice(73). Therefore,
542 results suggest that MyBP-C appears to plays a role in maintaining thick and thin filaments
543 near their equilibrium positions during contraction, possibly by linking thick and thin
544 filaments together. If so, then MyBP-C may promote efficient/strong cross-bridge binding
545 by maintaining alignment of binding sites relative to one another on thick and thin
546 filaments. Conversely, an increase in lattice disorder with loss of MyBP-C may lead to less
547 efficient binding of myosin cross-bridges and/or promote cross-bridge detachment,
548 thereby decreasing myosin duty ratio and increasing cycling rates(74, 75). The idea that
549 MyBP-C links thick and thin filaments together is also consistent with MyBP-C acting as a
550 drag force or internal load that slows cross-bridge cycling kinetics and relaxation(24, 45,
551 57).

552 MyBP-C also had significant effects on both the myosin head position and the thin filament.
553 The proportion of myosin heads in the ON state appeared unchanged following loss of
554 MyBP-C as indicated by the spacing of the M3 reflection (S_{M3})(Supplementary Fig. X3),
555 but the ordering of the myosin heads relative to the thick filament backbone was
556 significantly decreased at both SLs as indicated by a reduction in the M3 intensity (I_{M3})
557 (Fig. 6). Increased disorder of the myosin heads captured in the M3 intensity may be
558 indicative of less efficient cross-bridge binding to the thin filament and may explain the
559 faster cycling rates identified in mechanics experiments. Finally, loss of MyBP-C
560 decreased both the spacing of the third order troponin reflection (S_{T3}) and the spacing of
561 actin layer line 6 reflection (S_{ALL6}). The reduced spacing of these two actin-based
562 reflections indicate an overall reduction of thin filament length, consistent with the ability
563 of MyBP-C to bind to and exert a strain on the thin filament. In line with this, MyBP-C is
564 essential for thick filament stability and lattice rigidity(62, 63, 76). Notably, filament
565 compliance can affect stability of strongly bound cross-bridges and relaxation rates(77-
566 79). Taken together, the changes in X-ray diffraction reflections are consistent with a role
567 for MyBP-C in minimizing overall disorder of the sarcomere lattice during contraction and
568 maintaining myosin heads in ordered positions. Whereas proper alignment of thick and
569 thin filaments relative to one another may promote strong cross-bridge binding and cross-
570 bridge stability, loss of thick and thin filament alignment may promote cross-bridge
571 detachment, especially under strain.

572 **Limitations**

573 A limitation of our X-ray diffraction analysis was that structural changes were investigated
574 during isometric contraction, making it difficult to draw conclusions about whether dynamic
575 changes occur during rapid stretch that are not captured during steady state Ca^{2+}

576 activation. Future studies will include time-resolved X-ray diffraction measurements taken
577 as the muscle is being stretched in order to obtain structural information during the various
578 phases of the tension transient. Another limitation was that the soleus muscle contains a
579 mixed population of fast type and slow type fibers and we did not attempt to differentiate
580 their different contributions in mechanical force measurements. As a result, the
581 mechanical contribution of slow MyBP-C was likely underestimated due to the significant
582 presence of fast MyBP-C which was not subject to cleavage in $SpyC_1$ mice. In addition,
583 there are at least two splice variants of slow skeletal MyBP-C expressed in mouse and we
584 did not attempt to determine their relative expression(21).

585

586 **Conclusions**

587 Major conclusions from this study are that all 3 paralogs of MyBP-C (cardiac, fast skeletal
588 and slow skeletal) exert robust functional effects on force generation in their respective
589 muscle types. Using selective cleavage of each paralog we showed that all 3 had common
590 functional effects to increase Ca^{2+} sensitivity of tension and limit cross-bridge cycling rates
591 at submaximal levels of activation. In addition, all 3 were effective at damping force
592 oscillations that appeared following loss of MyBP-C when MyBP-C was cleaved with
593 TEVp. Finally, all 3 paralogs slowed strain-dependent cross-bridge detachment rates
594 which was evident as accelerated detachment rates (K_{rel}) and a lower force nadir (P_2)
595 following loss of MyBP-C when muscles were subjected to a rapid stretch. However, the
596 overall transient force response to a rapid stretch was unique in each muscle type and
597 dependent on the MyBP-C paralog expressed. In particular, MyBP-C paralogs uniquely
598 modulated strain dependence of cross-bridge detachment and thereby influenced SA
599 properties in each muscle type. This regulation of cross-bridge relaxation may have

600 significant physiological importance, as strain-induced cross-bridge shortening is key to
601 rapid relaxation at onset of diastole to allow for proper ventricular filling, and may also
602 enable rapid bursts in contraction in skeletal muscle.

603
604
605 **Materials and Methods**
606
607 Animal procedures:

608 All animal procedures were performed under protocols approved by the Institutional
609 Animal Care and Use Committee (IACUC) at the University of Arizona. $SpyC_1$, $SnoopC_2$,
610 and $SpyC_3$ (C57BL6/NJ) mice were created by the Genetically Engineered Mouse Models
611 (GEMM) core at the University of Arizona. All mice were bred and housed in a pathogen-
612 free barrier animal facility at the University of Arizona. Animal genotypes were confirmed
613 using PCR of DNA extracted from toe-clip samples and amplicons visualized on 1%
614 agarose gels.

615

616 Mice used in this study were euthanized via cervical dislocation following anesthesia with
617 isoflurane. Left ventricles, psoas, and soleus muscles were immediately dissected and
618 flash frozen in liquid nitrogen for long-term storage at -80°C for force measurements. For
619 X-ray diffraction measurements, muscles were permeabilized using glyercol (1:1
620 rigor:glycerol where Rigor solution contained (in mM): KCl (100), $MgCl_2$ (2),
621 ethyleneglycol-bis(β-aminoethyl)-N,N,N',N'-tetraacetic acid (EGTA, 5), Tris (10),
622 dithiothreitol (DTT, 1), 1:100 HALT™ Protease Inhibitor Cocktail (ThermoFisher Scientific,
623 Waltham, MA, USA)) at 4°C for 48 hours. After 48 hours the solution was refreshed and
624 then muscles were stored up to 60 days at -20°C until use.

625

626 Recombinant protein expression and purification:

627 Protein plasmids with desired DNA sequences were purchased from Genscript
628 (Piscataway, NJ, USA). BL21 and DE3 competent cells (C2527, New England Biolabs,
629 Ipswich, MA, USA) were transfected with plasmid DNA and protein purification was
630 performed as described previously.(13, 22)

631

632 Muscle force measurements:

633 Tissue was thawed in a skinning solution consisting of a Relax Buffer containing 1% Triton
634 X-100, 0.1% Saponin, and 1:100 HALT™ Protease Inhibitor Cocktail (ThermoFisher
635 Scientific, Waltham, MA, USA). Relax buffer contained (in mM): 100 KCl, 10 imidazole, 2
636 EGTA, 5 $MgCl_2$, 4 ATP (A2383, Sigma, St. Louis, MO, USA), and 1:100 HALT™ Protease
637 Inhibitor Cocktail at pH of 7.0. Multicellular preparations of cardiac cells and skeletal
638 muscle fibers were then isolated by mechanical disruption using a homogenizer (Omni
639 International 60CE54. Model: TH115). After homogenization, cardiac and skeletal muscle
640 cells were incubated with rotation in a skinning solution at 4°C for 15 and 30 min,
641 respectively. Detergent-permeabilized cardiac and skeletal muscle cells were then
642 washed thoroughly with fresh Relax buffer to remove residual detergents. Next, cardiac
643 cells and skeletal muscle fibers (~80-200 mm in length, 50-100 mm in width) were selected
644 and attached to a high-speed positional motor (Model: 315C-I, Aurora Scientific Inc.,
645 Aurora, Ontario, Canada) and a force transducer (Model 403 A series, Aurora Scientific
646 Inc., Aurora, Ontario, Canada) using aquarium sealant (Marineland, 100% clear silicone
647 rubber or Loctite, Clear Silicone Waterproof Multipurpose Adhesive Sealant). The

648 positional motor and force transducer were attached over a temperature-adjustable 8-well
649 platform (Model 803B, Aurora Scientific Inc., Aurora, Ontario, Canada) regulated by a
650 thermocouple (825A, Aurora Scientific Inc., Aurora, ON, Canada). The 8-well platform was
651 then mounted on the stage of an inverted light microscope (Model IX-53, Olympus
652 Instrument Co., Japan). The aquarium sealant was allowed to cure for 30 min before the
653 experiment was started. SL was then measured using video imaging in passive conditions
654 (at pCa 9.0) and SL was set to a final length of 2.3 μm and 2.4 μm for cardiac and skeletal
655 muscle, respectively. All muscle force measurements were obtained at 15°C using a range
656 of pCa solutions with free Ca^{2+} pCa 9.0 to 4.5, where pCa = -log[Ca^{2+}]. Force
657 measurements (F) recorded at each submaximal pCa solution were normalized to the
658 maximal force (F_0) at pCa 4.5 and to cross-sectional area of the muscle fiber assuming
659 circular dimensions. Data was fitted using a sigmoidal four-parameter logistic curve within
660 Graphpad Prism. k_{tr} was assessed by performing a slack-restretch test, where the muscle
661 was shortened to 80% of its reference length for 20 ms, stretched to 105% reference
662 length for 5 ms and returned to reference length. Tension transient parameters were
663 assessed by performing a rapid 2% stretch over 5 ms and held for 3 s. Cross-bridge
664 cycling rates (k_{tr} and shortening induced k_{df}) and cross-bridge relaxation (k_{rel}), were fit
665 using a single exponential curve and normalized to maximal rate (k_0) at pCa 4.5 and
666 plotted against isometric force.

667

668 N-terminal MyBP-C cleavage and *in situ* paste of recombinant proteins:

669 Mechanics experiments typically consisted of 3 consecutive sets of measurements: First,
670 before N-terminal cleavage of MyBP-C (control), second, after N-terminal cleavage of

671 MyBP-C with TEVp, and third in a subset of experiments after *in situ* paste of recombinant
672 MyBP-C. Proteolytic cleavage of domains C0-C7 in cardiac cells and C1-C7 in skeletal
673 muscle cells was performed by incubating myocytes in 20 μM AcTEV™ Protease
674 (ThermoFisher, 12575015) at 25°C for 30 min while the permeabilized muscle preparation
675 was attached to the high-speed positional motor and force transducer. After TEVp
676 incubation, cells were rigorously washed in fresh relax buffer (3 x for 3 min) to remove
677 TEV protease as well as cleaved endogenous MyBP-C N-terminal domains. Paste of
678 recombinant protein was done by incubating permeabilized cell preparations for 15 min at
679 15°C with 20 μM recombinant protein of choice containing a SpyCatcher sequence.
680 Myocytes were then washed (3 x for 3 min) using fresh relax buffer to remove excess
681 (non-ligated) recombinant protein. N-terminal MyBP-C cleavage and protein ligation was
682 assessed using SDS-PAGE gel electrophoresis and western blot as described
683 previously(23).

684 Small angle X-ray diffraction:

685 All X-ray diffraction experiments were performed with the small-angle instrument at the
686 BioCAT beamline 18ID at the Advanced Photon Source, Argonne National Laboratory.
687 Muscle experiments were performed both before and after the facility wide upgrade of
688 the Advanced Photon Source with changes to beam flux (Pre: ~$3x10^{12}$, Post: ~$5x10^{13}$
689 photons per second). The X-ray diffraction beam (0.103 nm wavelength), focusing at the
690 detector plane (Pre: ~0.06 x 0.15 mm. Post: 0.02 x 0.02 mm), sample to detector
691 distance (~2m), and detector (Mar 165, Rayonix Inc., USA) are identical to our previous
692 study in relaxed muscle fibers(23). An in-line camera was present to properly target
693 beam onto muscle fibers and assess for any irregularities in attachment of the muscle.
694 Muscle fibers were attached to custom fabricated clamps and connected to a high-speed

695 length controller (322C, Aurora Scientific, Canada) and a force transducer (402A, Aurora
696 Scientific, Canada) with a sampling rate of 1,000 Hz. Measurements from the force
697 transducer to identify activation levels of the fibers were visualized using Real Time
698 Muscle Data Acquisition and Analysis system (600A, Aurora Scientific, Canada).
699 Experiments were performed at ~25°C. SL was set at SL 2.4 μm or SL 3.0 μm using a 4-
700 mW Helium-Neon laser based on width of the first-order diffraction. Muscles were
701 activated by removal of relaxing solution (in mM: potassium propionate (45.3), N,N-
702 Bis(2-hydroxyethyl)-2-aminoethanesulfonic acid BES (40); EGTA (10), $MgCl_2$ (6.3), Na-
703 ATP (6.1), DTT (10), protease inhibitors [Complete], pH 7.0), three 30 second
704 incubations with pre-activating solution (in mM: potassium propionate (45.3), N,N-Bis(2-
705 hydroxyethyl)-2-aminoethanesulfonic acid BES (40); $MgCl_2$ (6.3), Na-ATP (6.1), DTT
706 (10), protease inhibitors [Complete], pH 7.0), and finally by incubation with pCa 6.0
707 solution (in mM: potassium propionate (170), magnesium acetate (2.5), MOPS (10) and
708 ATP (2.5), and CaEGTA and K_2EGTA were mixed at different proportions to obtain
709 different pCa ($-\log[Ca^{2+}]$), pH 7.0) values. Following incubation with pCa 6.0, tension
710 was monitored until the muscle reached a steady-state level of force, upon which the
711 bath was lowered with a servo-motor and X-ray images were taken in open air. No part
712 of the sample was exposed to the X-ray beam more than once. Samples then underwent
713 TEVp protease incubation as described above, and the process was repeated.

714 X-ray Diffraction Analysis:

715 Analysis of x-ray diffraction patterns was performed using MuscleX (version 1.22.0)
716 open-source data reduction and analysis package (BioCAT, Argonne National
717 Laboratories) as previously described(23, 80).

718 Statistics:

Statistical analyses were performed either in Graphpad Prism or JMP Pro (V16, SAS Institute Inc., Cary, NC, USA). All measurements reported as the mean ± SEM. Repeated measures one-way ANOVA tests with main effects pCa, TEVp treatment, and their interaction, as well as an individual fiber random effect were performed on measurements before TEV protease cleavage, after TEV protease cleavage, and when present, after addition of recombinant protein. A mixed effects test was used for any missing values. A paired t-test was used specifically to compare pCa50 values. The significance level was $p<0.05$. For additional statistical details see tables contained in Supplemental Dataset 1.

Acknowledgments

This research was performed on APS beam time award(s) from the Advanced Photon Source, a U.S. Department of Energy (DOE) Office of Science user facility operated for the DOE Office of Science by Argonne National Laboratory under Contract No. DE-AC02-06CH11357. BioCAT is supported by grant P30 GM138395 from the National Institute of General Medical Sciences of the National Institutes of Health. The content is solely the responsibility of the authors and does not necessarily reflect the official views of the National Institute of General Medical Sciences or the National Institutes of Health. We would like to thank Dr. Thomas C Irving for expertise and help with editing the manuscript and John Sullivan for generating a video of SPOC in soleus muscle. Funding for this study was provided by the National Institute of Health (HL080367 [SPH]), HL140925 [SPH], AR081935 [SPH], T32 HL007249 [NME]), the American Heart Association (827628 [NME]), and German Research Foundation (DFG) 454867250 to ALH.

References

1. L. Heling, M. A. Geeves, N. M. Kad, MyBP-C: one protein to govern them all. *J Muscle Res Cell Motil* **41**, 91–101 (2020).
2. D. Tamborrini *et al.*, Structure of the native myosin filament in the relaxed cardiac sarcomere. *Nature* **623**, 863–871 (2023).
3. D. Dutta, V. Nguyen, K. S. Campbell, R. Padron, R. Craig, Cryo-EM structure of the human cardiac myosin filament. *Nature* **623**, 853–862 (2023).
4. M. V. Razumova, K. L. Bezold, A. Y. Tu, M. Regnier, S. P. Harris, Contribution of the myosin binding protein C motif to functional effects in permeabilized rat trabeculae. *J Gen Physiol* **132**, 575–585 (2008).

757 5. A. E. Whitten, C. M. Jeffries, S. P. Harris, J. Trewhella, Cardiac myosin-binding protein C
758 decorates F-actin: implications for cardiac function. *Proc Natl Acad Sci U S A* **105**, 18360–
759 18365 (2008).
760 6. G. Kunst *et al.*, Myosin binding protein C, a phosphorylation-dependent force regulator
761 in muscle that controls the attachment of myosin heads by its interaction with myosin
762 S2. *Circ Res* **86**, 51–58 (2000).
763 7. A. Ababou, M. Gautel, M. Pfuhl, Dissecting the N-terminal myosin binding site of human
764 cardiac myosin-binding protein C. Structure and myosin binding of domain C2. *J Biol*
765 *Chem* **282**, 9204–9215 (2007).
766 8. C. Risi *et al.*, N-Terminal Domains of Cardiac Myosin Binding Protein C Cooperatively
767 Activate the Thin Filament. *Structure* **26**, 1604–1611 e1604 (2018).
768 9. J. Y. Mun *et al.*, Myosin-binding protein C displaces tropomyosin to activate cardiac thin
769 filaments and governs their speed by an independent mechanism. *Proc Natl Acad Sci U S*
770 *A* **111**, 2170–2175 (2014).
771 10. S. Nelson, S. Beck-Previs, S. Sadayappan, C. Tong, D. M. Warshaw, Myosin-binding
772 protein C stabilizes, but is not the sole determinant of SRX myosin in cardiac muscle. *J*
773 *Gen Physiol* **155** (2023).
774 11. J. W. McNamara *et al.*, Ablation of cardiac myosin binding protein-C disrupts the super-
775 relaxed state of myosin in murine cardiomyocytes. *J Mol Cell Cardiol* **94**, 65–71 (2016).
776 12. C. Y. Doh *et al.*, Molecular characterization of linker and loop-mediated structural
777 modulation and hinge motion in the C4-C5 domains of cMyBPC. *J Struct Biol* **214**,
778 107856 (2022).
779 13. A. C. Greenman, R. L. Sadler, S. P. Harris, Autoinhibition of cMyBP-C by its middle
780 domains. *J Mol Cell Cardiol* **200**, 82–92 (2025).
781 14. A. A. Glazier, A. Thompson, S. M. Day, Allelic imbalance and haploinsufficiency in
782 MYBPC3-linked hypertrophic cardiomyopathy. *Pflugers Arch* **471**, 781–793 (2019).
783 15. S. P. Harris, R. G. Lyons, K. L. Bezold, In the thick of it: HCM-causing mutations in myosin
784 binding proteins of the thick filament. *Circ Res* **108**, 751–764 (2011).
785 16. A. S. Helms *et al.*, Spatial and Functional Distribution of MYBPC3 Pathogenic Variants
786 and Clinical Outcomes in Patients With Hypertrophic Cardiomyopathy. *Circ Genom*
787 *Precis Med* **13**, 396–405 (2020).
788 17. C. A. Gurnett *et al.*, Myosin binding protein C1: a novel gene for autosomal dominant
789 distal arthrogryposis type 1. *Hum Mol Genet* **19**, 1165–1173 (2010).
790 18. J. W. McNamara, S. Sadayappan, Skeletal myosin binding protein-C: An increasingly
791 important regulator of striated muscle physiology. *Arch Biochem Biophys* **660**, 121–128
792 (2018).
793 19. J. M. Mariano *et al.*, Pulsatile Myofilament Activity in Myotrem Myopathy Associated
794 with Myogenic Tremor. *Int J Mol Sci* **26** (2025).
795 20. C. E. Oakley, B. D. Hambly, P. M. Curmi, L. J. Brown, Myosin binding protein C: structural
796 abnormalities in familial hypertrophic cardiomyopathy. *Cell Res* **14**, 95–110 (2004).
797 21. M. A. Ackermann, A. Kontrogianni-Konstantopoulos, Myosin binding protein-C slow: a
798 multifaceted family of proteins with a complex expression profile in fast and slow twitch
799 skeletal muscles. *Front Physiol* **4**, 391 (2013).
800 22. N. C. Napierski *et al.*, A Novel "Cut and Paste" Method for In Situ Replacement of
801 cMyBP-C Reveals a New Role for cMyBP-C in the Regulation of Contractile Oscillations.
802 *Circ Res* **126**, 737–749 (2020).

803 23. A. L. Hessel *et al.*, Myosin-binding protein C regulates the sarcomere lattice and
804 stabilizes the OFF states of myosin heads. *Nat Commun* **15**, 2628 (2024).
805 24. A. V. Dvornikov, S. P. Harris, Myosin-binding protein C slows cardiac myofibril relaxation
806 kinetics. *J Physiol* **603**, 5351–5368 (2025).
807 25. B. Zakeri *et al.*, Peptide tag forming a rapid covalent bond to a protein, through
808 engineering a bacterial adhesin. *Proc Natl Acad Sci U S A* **109**, E690–697 (2012).
809 26. G. Veggiani *et al.*, Programmable polyproteams built using twin peptide superglues. *Proc*
810 *Natl Acad Sci U S A* **113**, 1202–1207 (2016).
811 27. B. Brenner, E. Eisenberg, Rate of force generation in muscle: correlation with
812 actomyosin ATPase activity in solution. *Proc Natl Acad Sci U S A* **83**, 3542–3546 (1986).
813 28. G. K. Dhoot, M. C. Hales, B. M. Grail, S. V. Perry, The isoforms of C protein and their
814 distribution in mammalian skeletal muscle. *J Muscle Res Cell Motil* **6**, 487–505 (1985).
815 29. J. E. Wolfe *et al.*, SPontaneous Oscillatory Contraction (SPOC): auto-oscillations observed
816 in striated muscle at partial activation. *Biophys Rev* **3**, 53–62 (2011).
817 30. A. F. Huxley, R. M. Simmons, Proposed mechanism of force generation in striated
818 muscle. *Nature* **233**, 533–538 (1971).
819 31. L. E. Ford, A. F. Huxley, R. M. Simmons, Tension responses to sudden length change in
820 stimulated frog muscle fibres near slack length. *J Physiol* **269**, 441–515 (1977).
821 32. J. S. Davis, N. D. Epstein, Kinetic effects of fiber type on the two subcomponents of the
822 Huxley-Simmons phase 2 in muscle. *Biophys J* **85**, 390–401 (2003).
823 33. J. E. Stelzer, R. L. Moss, Contributions of stretch activation to length-dependent
824 contraction in murine myocardium. *J Gen Physiol* **128**, 461–471 (2006).
825 34. C. R. Straight, K. M. Bell, J. N. Slosberg, M. S. Miller, D. M. Swank, A myosin-based
826 mechanism for stretch activation and its possible role revealed by varying phosphate
827 concentration in fast and slow mouse skeletal muscle fibers. *Am J Physiol Cell Physiol*
828 **317**, C1143–C1152 (2019).
829 35. M. Linari, M. K. Reedy, M. C. Reedy, V. Lombardi, G. Piazzesi, Ca-activation and stretch-
830 activation in insect flight muscle. *Biophys J* **87**, 1101–1111 (2004).
831 36. J. O. Vigoreaux, J. Vigoreaux, SpringerLink (2006) Nature's versatile engine : insect flight
832 muscle inside and out. in *Molecular Biology Intelligence Unit* (Landes
833 Bioscience/Eurekah.com

834 Springer Science+Business Media

835 Springer US, Georgetown, Tex

836 New York, N.Y

837 New York, NY).
838 37. R. Rice *et al.*, Cardiac myosin heavy chain isoform exchange alters the phenotype of
839 cTnT-related cardiomyopathies in mouse hearts. *J Mol Cell Cardiol* **48**, 979–988 (2010).
840 38. B. C. Tanner, Y. Wang, J. Robbins, B. M. Palmer, Kinetics of cardiac myosin isoforms in
841 mouse myocardium are affected differently by presence of myosin binding protein-C. *J*
842 *Muscle Res Cell Motil* **35**, 267–278 (2014).
843 39. R. Mamidi, K. S. Gresham, S. Verma, J. E. Stelzer, Cardiac Myosin Binding Protein-C
844 Phosphorylation Modulates Myofilament Length-Dependent Activation. *Front Physiol* **7**,
845 38 (2016).

846 40. W. Ma, T. C. Irving, Small Angle X-ray Diffraction as a Tool for Structural Characterization
847 of Muscle Disease. *Int J Mol Sci* **23** (2022).
848 41. A. L. Hessel *et al.*, The distinctive mechanical and structural signatures of residual force
849 enhancement in myofibers. *Proc Natl Acad Sci U S A* **121**, e2413883121 (2024).
850 42. V. Joumaa *et al.*, Effect of Active Lengthening and Shortening on Small-Angle X-ray
851 Reflections in Skinned Skeletal Muscle Fibres. *Int J Mol Sci* **22** (2021).
852 43. G. Piazzesi *et al.*, Changes in conformation of myosin heads during the development of
853 isometric contraction and rapid shortening in single frog muscle fibres. *J Physiol* **514 (Pt
854 2)**, 305–312 (1999).
855 44. H. E. Huxley, W. Brown, The low-angle x-ray diagram of vertebrate striated muscle and
856 its behaviour during contraction and rigor. *J Mol Biol* **30**, 383–434 (1967).
857 45. F. S. Korte, K. S. McDonald, S. P. Harris, R. L. Moss, Loaded shortening, power output,
858 and rate of force redevelopment are increased with knockout of cardiac myosin binding
859 protein-C. *Circ Res* **93**, 752–758 (2003).
860 46. T. Song *et al.*, Fast skeletal myosin-binding protein-C regulates fast skeletal muscle
861 contraction. *Proc Natl Acad Sci U S A* **118** (2021).
862 47. K. Sato, M. Ohtaki, Y. Shimamoto, S. Ishiwata, A theory on auto-oscillation and
863 contraction in striated muscle. *Prog Biophys Mol Biol* **105**, 199–207 (2011).
864 48. T. Kagemoto, A. Li, C. Dos Remedios, S. Ishiwata, Spontaneous oscillatory contraction
865 (SPOC) in cardiomyocytes. *Biophys Rev* **7**, 15–24 (2015).
866 49. X. Li *et al.*, Two novel mutations in myosin binding protein C slow causing distal
867 arthrogryposis type 2 in two large Han Chinese families may suggest important
868 functional role of immunoglobulin domain C2. *PLoS One* **10**, e0117158 (2015).
869 50. K. Ha *et al.*, MYBPC1 mutations impair skeletal muscle function in zebrafish models of
870 arthrogryposis. *Hum Mol Genet* **22**, 4967–4977 (2013).
871 51. S. P. Harris, Making waves: A proposed new role for myosin-binding protein C in
872 regulating oscillatory contractions in vertebrate striated muscle. *J Gen Physiol* **153**
873 (2021).
874 52. J. C. Robinett, L. M. Hanft, B. Biesiadecki, K. S. McDonald, Molecular regulation of
875 stretch activation. *Am J Physiol Cell Physiol* **323**, C1728–C1739 (2022).
876 53. S. Galler, O. Andruchov, G. M. Stephenson, D. G. Stephenson, Qualitatively different
877 cross-bridge attachments in fast and slow muscle fiber types. *Biochem Biophys Res
878 Commun* **385**, 44–48 (2009).
879 54. P. C. Woods, D. M. Swank, M. S. Miller, Stretch activation combats force loss from
880 fatigue in fast-contracting mouse skeletal muscle fibers. *J Gen Physiol* **157** (2025).
881 55. B. M. Palmer *et al.*, Enhancing diastolic function by strain-dependent detachment of
882 cardiac myosin crossbridges. *J Gen Physiol* **152** (2020).
883 56. R. H. Abbott, G. J. Steiger, Temperature and amplitude dependence of tension transients
884 in glycerinated skeletal and insect fibrillar muscle. *J Physiol* **266**, 13–42 (1977).
885 57. J. C. Robinett, L. M. Hanft, J. Geist, A. Kontrogianni-Konstantopoulos, K. S. McDonald,
886 Regulation of myofilament force and loaded shortening by skeletal myosin binding
887 protein C. *J Gen Physiol* **151**, 645–659 (2019).
888 58. C. S. Chung, C. W. Hoopes, K. S. Campbell, Myocardial relaxation is accelerated by fast
889 stretch, not reduced afterload. *J Mol Cell Cardiol* **103**, 65–73 (2017).
890 59. J. I. Wakefield, S. P. Bell, B. M. Palmer, Inorganic phosphate accelerates cardiac
891 myofilament relaxation in response to lengthening. *Front Physiol* **13**, 980662 (2022).

892 60. R. Stehle *et al.*, Mechanical properties of sarcomeres during cardiac myofibrillar
893 relaxation: stretch-induced cross-bridge detachment contributes to early diastolic filling.
894 *J Muscle Res Cell Motil* **27**, 423–434 (2006).
895 61. C. Poggesi, C. Tesi, R. Stehle, Sarcomeric determinants of striated muscle relaxation
896 kinetics. *Pflugers Arch* **449**, 505–517 (2005).
897 62. B. M. Palmer *et al.*, Effect of cardiac myosin binding protein-C on mechanoenergetics in
898 mouse myocardium. *Circ Res* **94**, 1615–1622 (2004).
899 63. B. M. Palmer *et al.*, Roles for cardiac MyBP-C in maintaining myofilament lattice rigidity
900 and prolonging myosin cross-bridge lifetime. *Biophys J* **101**, 1661–1669 (2011).
901 64. B. C. W. Tanner, M. J. Previs, Y. Wang, J. Robbins, B. M. Palmer, Cardiac myosin binding
902 protein-C phosphorylation accelerates beta-cardiac myosin detachment rate in mouse
903 myocardium. *Am J Physiol Heart Circ Physiol* **320**, H1822–H1835 (2021).
904 65. Y. Hwang, T. Washio, T. Hisada, H. Higuchi, M. Kaya, A reverse stroke characterizes the
905 force generation of cardiac myofilaments, leading to an understanding of heart function.
906 *Proc Natl Acad Sci U S A* **118** (2021).
907 66. M. S. Woody, D. A. Winkelmann, M. Capitanio, E. M. Ostap, Y. E. Goldman, Single
908 molecule mechanics resolves the earliest events in force generation by cardiac myosin.
909 *Elife* **8** (2019).
910 67. J. W. Pringle, The excitation and contraction of the flight muscles of insects. *J Physiol*
911 **108**, 226–232 (1949).
912 68. G. J. Steiger, J. C. Ruegg, Energetics and "efficiency" in the isolated contractile machinery
913 of an insect fibrillar muscle at various frequencies of oscillation. *Pflugers Arch* **307**, 1–21
914 (1969).
915 69. T. P. Vu Manh *et al.*, Expression of cardiac myosin-binding protein-C (cMyBP-C) in
916 Drosophila as a model for the study of human cardiomyopathies. *Hum Mol Genet* **14**, 7–
917 17 (2005).
918 70. M. C. Reedy, B. Bullard, J. O. Vigoreaux, Flightin is essential for thick filament assembly
919 and sarcomere stability in Drosophila flight muscles. *J Cell Biol* **151**, 1483–1500 (2000).
920 71. B. Bullard, A. Pastore, Through thick and thin: dual regulation of insect flight muscle and
921 cardiac muscle compared. *J Muscle Res Cell Motil* **40**, 99–110 (2019).
922 72. K. B. Campbell, M. Chandra, Functions of stretch activation in heart muscle. *J Gen*
923 *Physiol* **127**, 89–94 (2006).
924 73. L. C. Yu, A. C. Steven, G. R. Naylor, R. C. Gamble, R. J. Podolsky, Distribution of mass in
925 relaxed frog skeletal muscle and its redistribution upon activation. *Biophys J* **47**, 311–
926 321 (1985).
927 74. T. L. Daniel, A. C. Trimble, P. B. Chase, Compliant realignment of binding sites in muscle:
928 transient behavior and mechanical tuning. *Biophys J* **74**, 1611–1621 (1998).
929 75. I. A. Telley, J. Denoth, E. Stussi, G. Pfitzer, R. Stehle, Half-sarcomere dynamics in
930 myofibrils during activation and relaxation studied by tracking fluorescent markers.
931 *Biophys J* **90**, 514–530 (2006).
932 76. L. R. Nyland *et al.*, Cardiac myosin binding protein-C is essential for thick-filament
933 stability and flexural rigidity. *Biophys J* **96**, 3273–3280 (2009).
934 77. K. S. Campbell, Filament compliance effects can explain tension overshoots during force
935 development. *Biophys J* **91**, 4102–4109 (2006).
936 78. B. Kiss *et al.*, Nebulin stiffens the thin filament and augments cross-bridge interaction in
937 skeletal muscle. *Proc Natl Acad Sci U S A* **115**, 10369–10374 (2018).

79. K. S. Campbell, Compliance Accelerates Relaxation in Muscle by Allowing Myosin Heads to Move Relative to Actin. *Biophys J* **110**, 661–668 (2016).
80. J. Jiratrakanvong *et al.*, MuscleX: data analysis software for fiber diffraction patterns from muscle. *J Synchrotron Radiat* **31**, 1401–1408 (2024).

Figures and Tables

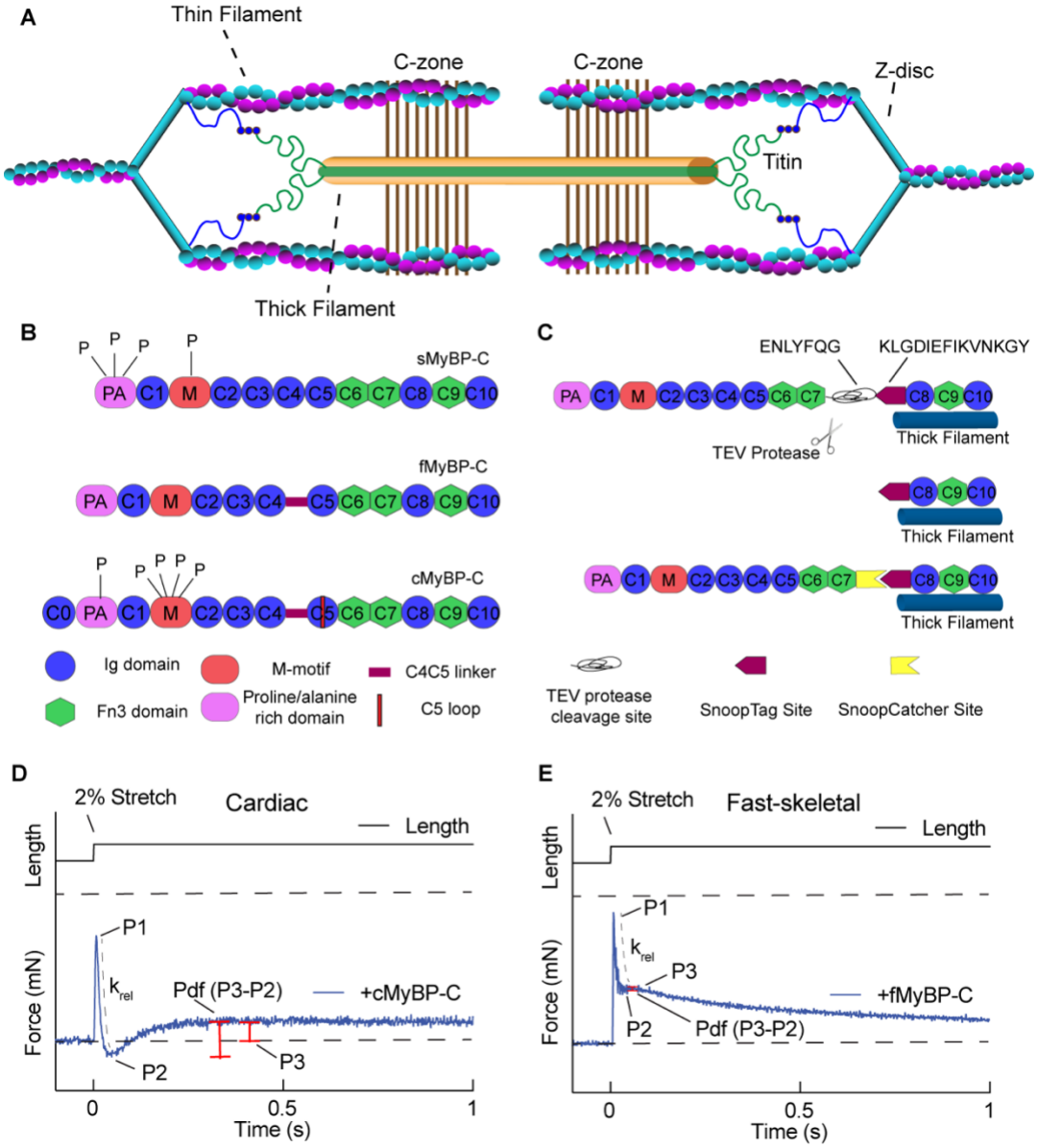

Figure 1: Sarcomere organization, MyBP-C structure, and utilization of the "cut-and-paste" mouse models to investigate muscle response to rapid stretch. A) Illustration of a muscle sarcomere highlighting Myosin Binding Protein-C location in the C-zone. B) Schematic of slow, fast skeletal, and cardiac Myosin Binding Protein-C paralogs. Slow and cardiac isoforms contain variable phosphorylation sites within the proline/alanine-rich as well as M-domain. Both fast and cardiac contain a linker between domains C4C5 while slow does not. Cardiac MyBP-C also contains an additional N-terminal immunoglobulin domain termed C0 as well as a 28 amino acid loop within the C5 domain. C) Schematic representation of the cut-and-paste system in fast skeletal Myosin Binding Protein-C. D) Representative force transient traces from cardiac and skeletal muscle highlighting shape differences and defining stretch activation terms for different muscle type.

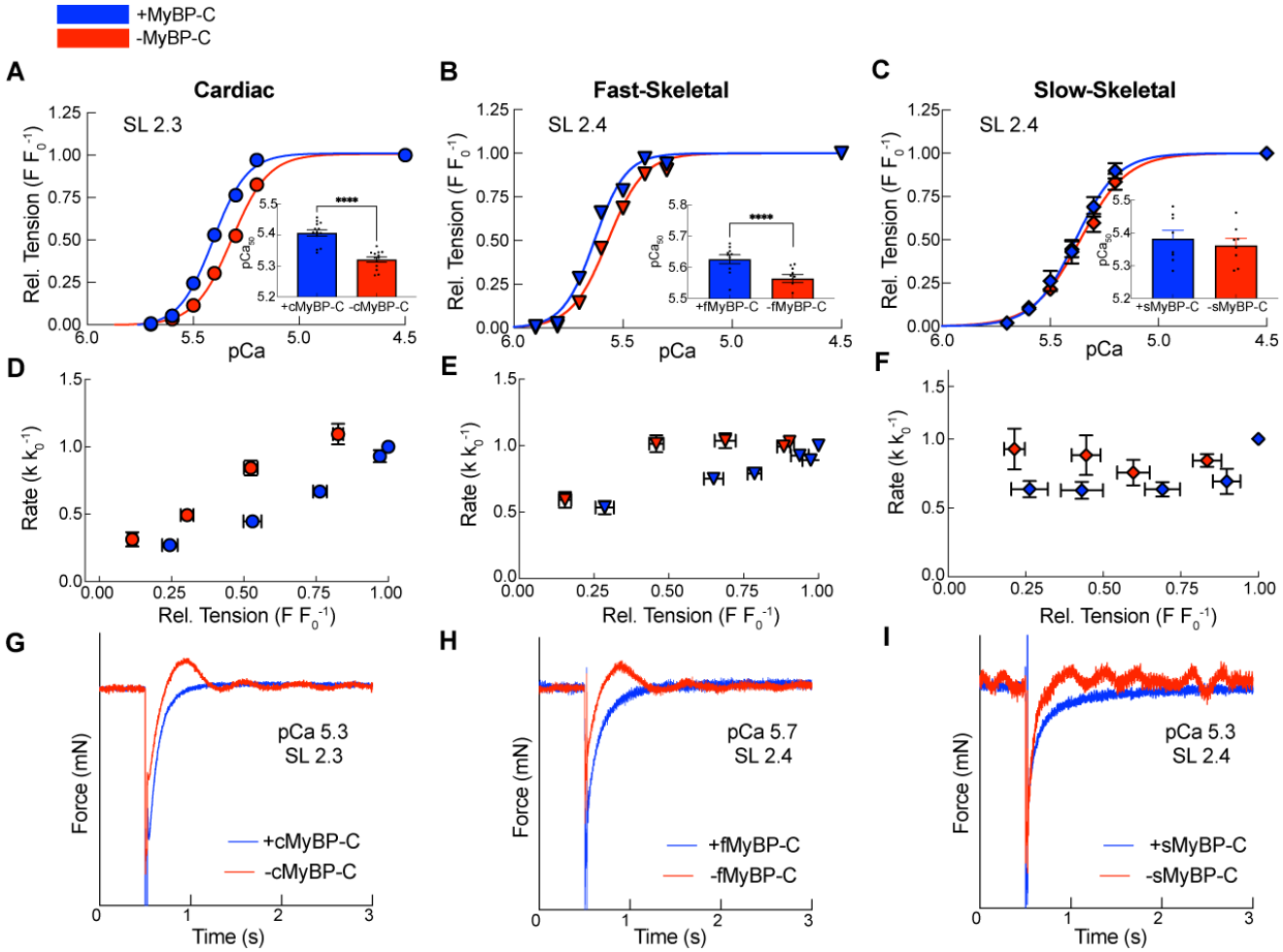

Figure 2: Removal of MyBP-C alters Ca^{2+}-sensitivity, cross-bridge cycling rates, and produces oscillatory contractions in each muscle type. A-C) Tension-pCa curves for cardiac (A), fast skeletal (B), and slow skeletal (C) before (blue) and after (red) removal of MyBP-C. D-F) Changes in cross-bridge cycling rates in cardiac (D), fast (E), and slow skeletal (F) before and after removal of MyBP-C. G-I) Representative force traces highlighting force overshoots and tension oscillations at steady-state force in cardiac (G), fast (H), and slow skeletal (I) before and after removal of MyBP-C. Force traces only in Figure 3i (sMyBP-C) were smoothed for clearer visualization of oscillations on Graphpad Prism. Data presented as mean ± s.e.m. pCa_{50} values assessed with paired t-test. **** = $p < 0.0001$ in (a-c). k_{tr} assessed with a two-way ANOVA with pCa and treatment as main effects also assessing their interaction. Individual fiber was included as a random effect. Treatment showed significance in (D-F) (D: Treatment: Prob > F = 0.0254, E: Treatment*pCa Prob > F = < 0.0033, F: Treatment Prob > F = 0.0038) A Student's t-test or Tukey Honestly Statistically Different (HSD) post-hoc test was performed on significant main effects ($p < 0.05$). Dataset from: Cardiac (n=13 cardiomyocytes. N=4 mice). Psoas (n=10 fibers. N=3 mice). Soleus (n=8. N=3 +sMyBP-C. N=4 -sMyBP-C). Figure 2B, 2E, and 2H are taken from Hessel et, al. 2024 publication in Nature Communications (23).

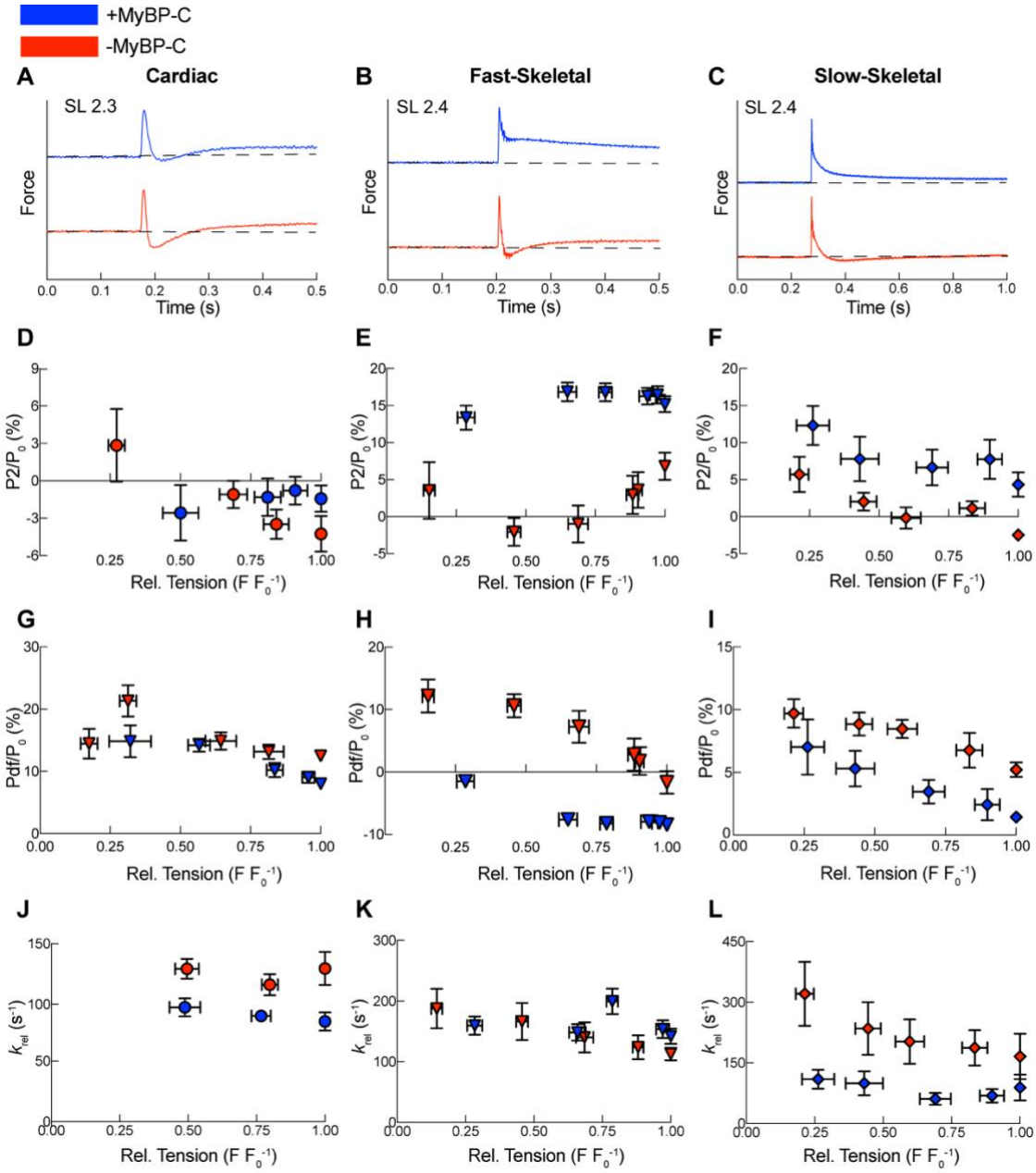

Figure 3: MyBP-C paralogs differentially affect tension transients following rapid stretch in each muscle type **a-c:** Representative force traces following 2% rapid stretch before (blue) and after (red)TEVp treatment of cardiac (a) fast skeletal psoas (b), and slow skeletal soleus (c). **d-f:** Mechanical measurements of the P_2 nadir before and after TEVp treatment in cardiac (d)(pCa*Treatment Prob > F = <0.0001, fast skeletal psoas (e) (Treatment Prob > F = <0.0001, and slow skeletal soleus (f) (n.s). **g-i:** Mechanical measurements of P_{df}, the amplitude of delayed force redevelopment, before and after TEVp treatment of cardiac (g)(Treatment Prob > F = 0.0001), fast skeletal psoas (h)(Treatment*pCa Prob > F = 0.0118), and slow skeletal soleus (i)(Treatment Prob > F = 0.006). **j-l:** Mechanical measurements of the rate of cross-bridge

1006 relaxation (k_{rel}) following rapid 2% stretch before and after TEVp treatment of cardiac (j)(Prob >
1007 F = <0.0001), fast skeletal psoas (k)(Treatment: Prob > F = 0.0272), and slow skeletal soleus
1008 (l)(n.s). Data presented as mean ± s.e.m. A repeated measures ANOVA design was performed
1009 throughout with pCa, treatment, and their interaction as main effects. A random effect was
1010 included for each individual fiber. A Student's t-test or Tukey's HSD post-hoc test was performed
1011 on significant main effects ($p < 0.05$). Dataset: Cardiac from (n=13 cardiomyocytes. N=4 mice).
1012 Psoas (n=10 fibers. N=3 mice). Soleus (n=8. N=3 +sMyBP-C. N=4 -sMyBP-C). Further detail in
1013 supplement.

1014

1015

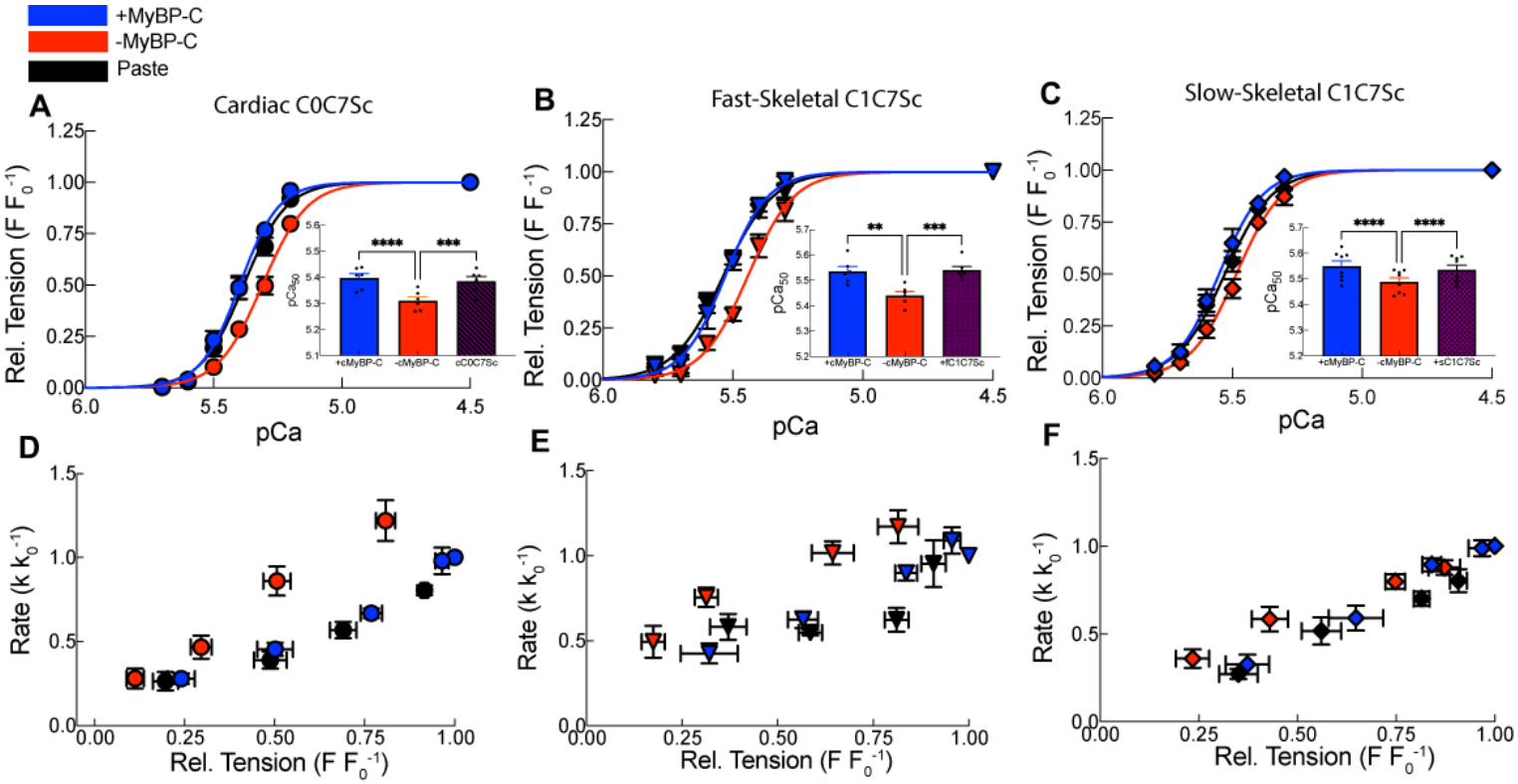

Figure 4: Cut-and-paste experiments performed in detergent permeabilized cardiac muscle to assess Ca^{2+}-sensitivity and k_{tr} after *in situ* replacement of recombinant cardiac, fast skeletal, and slow skeletal MyBP-C. **a-c:** Relative tension-pCa with inset containing average pCa_{50} following each curve for cC0C7Sc(a), fC1C7Sc (b), and sC1C7Sc (c). ** = p = <0.0001, *** p < 0.0005, **** p = <0.005 **d-f:** Changes in k_{tr} before and after removal of endogenous cMyBP-C and following paste of cC0C7Sc (d) (pCa*Treatment Prob > F = 0.0046), fC1C7Sc (e) (Treatment Prob > F = 0.0061) and sC1C7Sc (f) (Treatment Prob > F = 0.0046). Statistics throughout are an ANOVA design with pCa, treatment, and their interaction as main effects, as well as an individual fiber random effect. Statistically significant differences were assessed using a Tukey's HSD post-hoc test on statistically significant differences (p < 0.05). Dataset: cC0C7Sc (n=7, N=3), fC1C7Sc (n=6, N=5), sC1C7Sc (n=8, N=6).

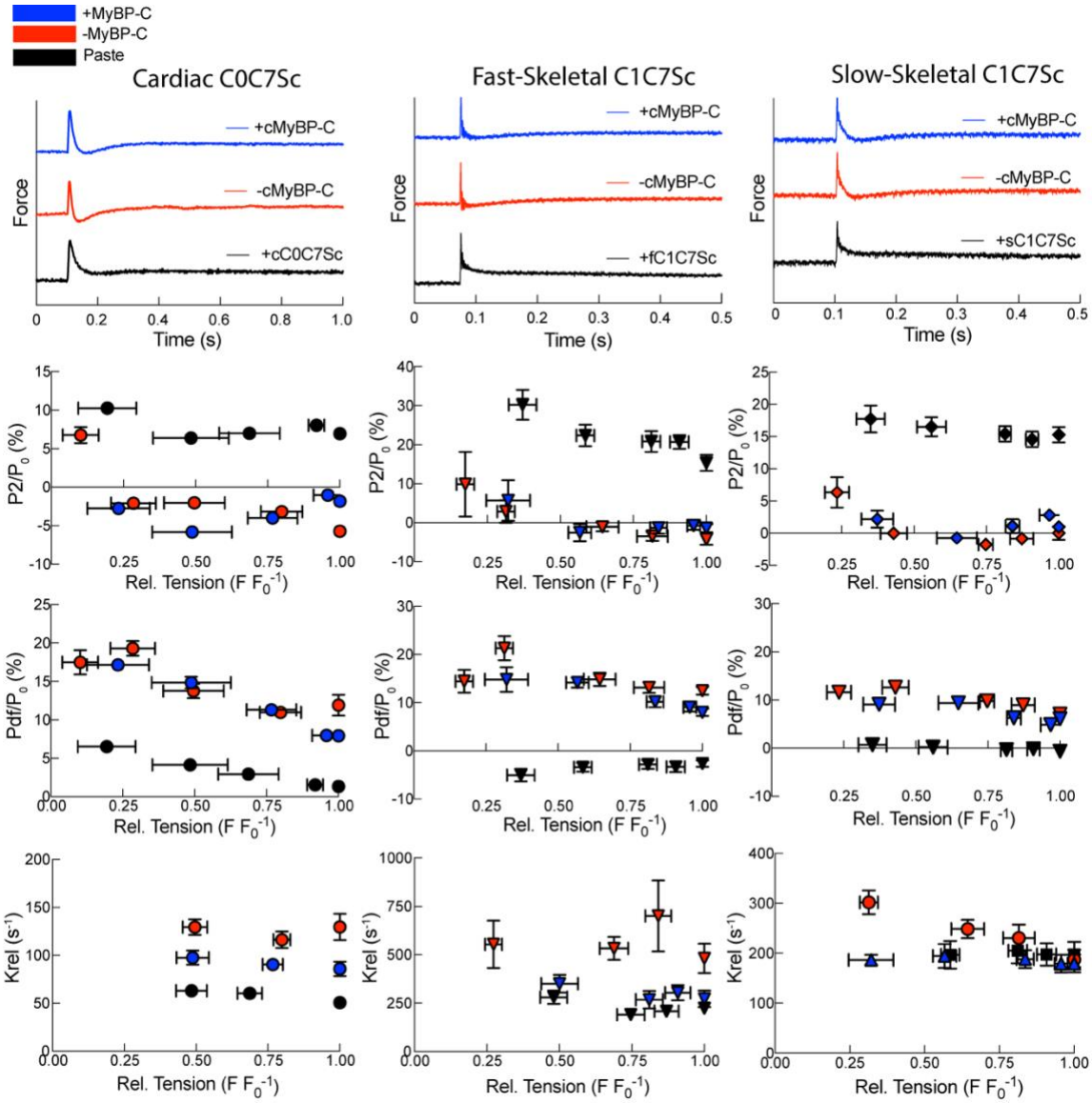

Figure 5: Amplitudes of strain-induced cross-bridge detachment (P_2), stretch activation (P_{df}), and cross-bridge relaxation kinetics (k_{rel}) in cardiac muscle following *in situ* replacement with cC0C7Sc, fC1C7Sc, and sC1C7Sc. **a-c:** Representative force traces of cardiac tension transients before (blue) and after (red) removal of endogenous cMyBP-C, and following replacement (black) with recombinant cC0C7Sc (a) fC1C7Sc (b), and sC1C7Sc (c). **d-f:** Amplitude of strain induced cross-bridge detachment (P_2) before and after removal of endogenous cMyBP-C and after replacement with cC0C7Sc (d) (pCa*Treatment*pCa Prob > F = <0.0001), fC1C7Sc (e) (Treatment Prob > F = <0.0001), and sC1C7Sc (f))(Treatment*pCa Prob > F = 0.0234) **g-i:** Amplitude of stretch activation (P_{df}) before and after removal of endogenous cMyBP-C and after *in situ* replacement with cC0C7Sc (g)(Treatment*pCa Prob > F = 0.0029), fC1C7Sc (h)(Treatment*pCa Prob > F = 0.0076), and sC1C7Sc (i)(Treatment*pCa Prob>F = 0.0181. **j-l:** Rates of stretch induced cross-bridge relaxation (k_{rel}) before and after removal of endogenous

1047 cMyBP-C and after *in situ* replacement with cC0C7Sc (j)(Treatment Prob > F = <0.0001), fC1C7Sc
1048 (k)(Treatment Prob > F = <0.0001), and sC1C7Sc (l)(Treatment*pCa Prob > F = 0.0076). Statistics
1049 throughout are an ANOVA design with pCa, treatment, and their interaction as main effects,
1050 including an individual fiber random effect. A post-hoc Tukey's HSD test was performed on
1051 statistically different main effects ($p < 0.05$). Dataset: cC0C7Sc (n=7, N=3), fC1C7Sc (n=6, N=5),
1052 sC1C7Sc (n=8, N=6).

1053

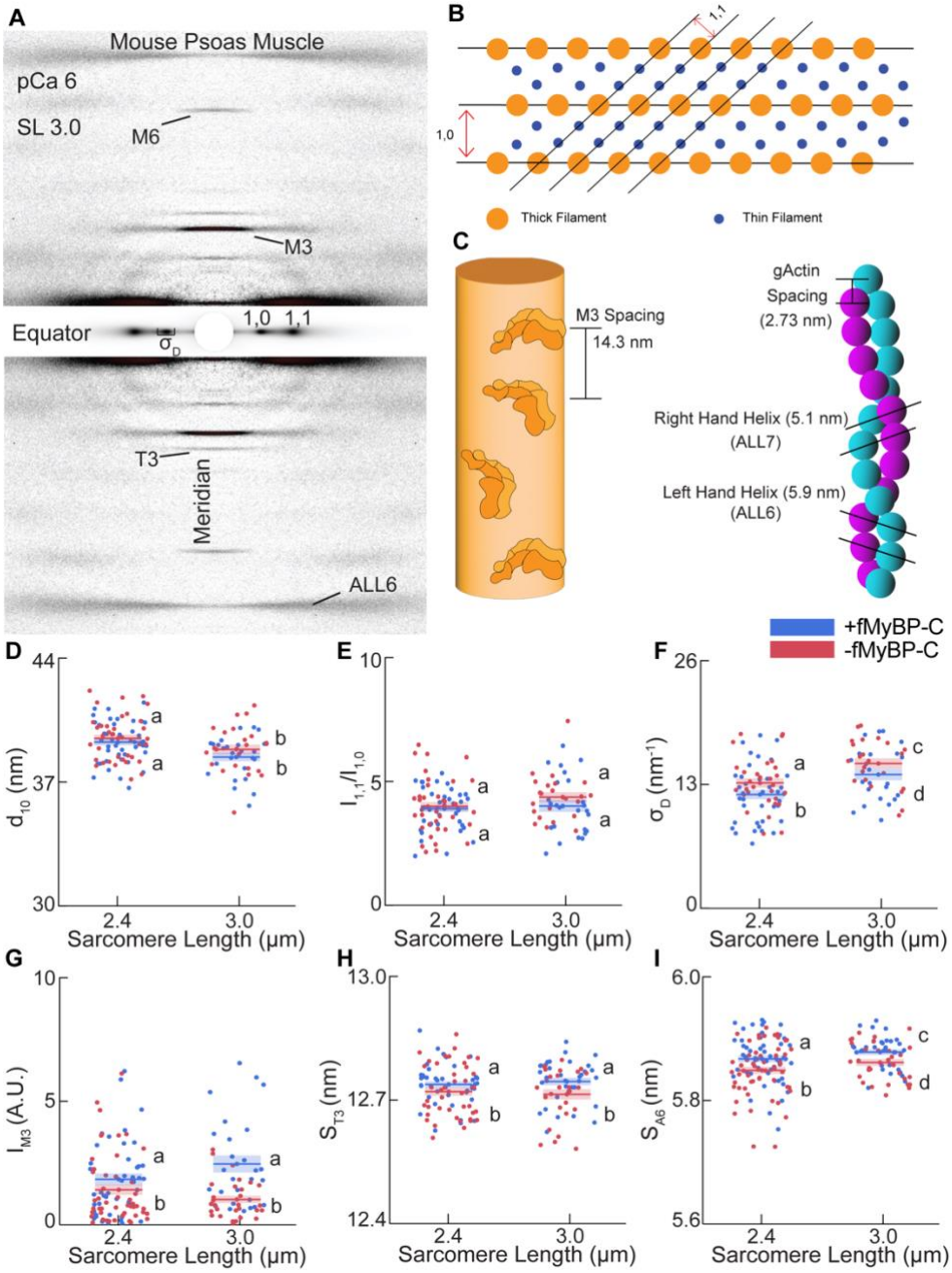

Figure 6: Equatorial and meridional reflections of isometrically contracting psoas Muscle in presence and absence of fMyBP-C. **a)** Representative X-ray diffraction image at SL 3.0 and pCa 6.0 highlighting meridional reflections (M3, T3, M6, A6) assessed in this study. **b)** Graphic showing a cross-sectional view of the sarcomere lattice as well as important equatorial reflections. **c) Left:** Schematic of the quasi-helical arrangement of myosin heads on the thick filament backbone, where the M3 reflection is highlighted as difference in space between individual myosin crowns. **Right:** Schematic of the thin filament, highlighting both the left-handed and right-handed helix of the actin monomers and their spacings. **d)** Lattice spacing of permeabilized psoas muscle at SL 2.4 and SL 3.0 before and after removal of fMyBP-C (Treatment: Prob > F 0.1494) **e)** I_{11}/I_{10} intensity ratio of permeabilized psoas muscle at SL 2.4 and

30 before and after removal of fMyBP-C. (Treatment: Prob > F = 0.2284) **f)** Heterogeneity of lattice spacing (σ_D) of permeabilized psoas muscle at SL 2.4 and 3.0 before and after removal of fMyBP-C. (Treatment: Prob > F = 0.003) **g)** Intensity of the M3 reflection (I_{M3}) of permeabilized psoas muscle at SL 2.4 and 3.0 before and after removal of fMyBP-C. (Treatment: Prob > F = 0.0001) **h)** T3 spacing (S_{T3}) of permeabilized psoas muscle at pCa 6.0 at SL 2.4 and 3.0 before and after removal of fMyBP-C. (Treatment: Prob > F = 0.0377) **i)** Actin layer line 6 spacing (S_{ALL6}) of permeabilized psoas muscle at SL 2.4 and 3.0 before and after removal of fMyBP-C. (Treatment: Prob > F = 0.0026) Statistics throughout are a repeated measure ANOVA design with SL, treatment, and their interaction as main effects, including a random effect on individual fiber. A Student's t-test or Tukey's HSD Post-Hoc test was performed on statistically significant differences and presented in figures as connecting letters. Dataset: (n=43 fibers, N=13 animals).